An integrated predictive energy management for light-duty range-extended plug-in fuel cell electric vehicle

Yang Zhou, Huan Li, Alexandre Ravey, Marie-Cécile Péra

An Integrated Predictive Energy Management for Light-Duty Range-Extended Plug-in Fuel Cell Electric Vehicle

Yang Zhou*[1], Huan Li[2], Alexandre Ravey[1], Marie-Cécile Péra[1]

[1]FEMTO-ST (UMR CNRS 6174), FCLAB (FR CNRS 3539), Univ. Bourgogne Franche-Comté, UTBM BELFORT, FRANCE.

[2]Univ. Normandie, UNICAEN, LUSAC, CHERBOURG, FRANCE.

yang.zhou@utbm.fr; huan.li@unicaen.fr; alexandre.ravey@utbm.fr; marie-cecile.pera@univ-fcomte.fr.

* *Corresponding Author.*

Abstract

A reliable power distribution strategy is of great significance towards the performance enhancement of fuel cell electric vehicles. In this work, a novel model predictive control-based energy management is developed for a fuel cell based light-duty range-extended hybrid electric vehicle. To fulfill the model predictive control framework, a cooperative speed forecasting method based on Markov Chain and fuzzy C-means clustering technique is proposed, which contains multiple predictive sub-models for handling different driving patterns. The final prediction results are obtained by synthesizing the forecasted speed profiles from all sub-models with the quantified fuzzy membership degrees. Besides, an adaptive battery State-of-Charge reference generator is built, which can regulate the SoC depleting rates against various power requirements. Combined with the forecasted speed and SoC reference, the desirable control actions are derived through minimizing the performance index over each finite time horizon. As a result, under the realistic urban-based postal-delivery mission profiles, the proposed strategy can achieve over 3.79% equivalent hydrogen consumption saving and over 40.04% fuel cell power dynamics decrement against benchmark strategy. Moreover, the presented predictive energy management is robust to certain level of trip duration estimation errors, further indicating its suitability for real applications.

Key words: ***Energy Management Strategy, Multi-objective Optimization, Velocity Forecasting, PHEV, Fuel Cell.***

Nomenclature

ABBREVIATIONS

EMS	Energy Management Strategy
FCPHEV	Fuel Cell Plug-in Hybrid Electric Vehicles
MPC	Model Predictive Control
SoC	State-of-Charge
PHEV	Plug-in Hybrid Electric Vehicles
PEMFC	Proton Exchange Membrane Fuel Cell
ICE	Internal Combustion Engine
HEV	Hybrid Electric Vehicles
FCS	Fuel Cell System
DP	Dynamic Programming
PMP	Pontryagin's Minimum Principle
GA	Genetic Algorithm
ECMS	Equivalent Consumption Minimization Strategy
FC	Fuel Cell
MC	Markov Chain
NN	Neural Network
PEMS	Predictive Energy Management Strategy
CD-CS	Charge-Depleting Charge-Sustaining
RBF	Radial Basis Function
TPM	Transition Probability Matrix
BPNN	Back Propagation Neural Network
SQP	Sequential Quadratic Programming
RMSE	Root Mean Square Errors
MSMC	Multi-Step Markov Chain
ITS	Intelligent Transportation Systems
GPS	Global Positioning Systems
L-MPC	Model Predictive Control with Linear SoC reference
A-MPC	Model Predictive Control with Adaptive SoC reference
EM	Electrical Machine
FCM-MC	Fuzzy C-means enhanced Markov Chain predictor
OCV	Open-circuit voltage

SYMBOLS

m_v	Vehicle mass
v	Vehicle speed
P_{pro}	Propulsion power demand
P_{FC}	PEMFC system net power
P_{BAT}	Battery power
P_d	DC bus power demand
c_r	Rolling resistance coefficient
g	Gradational acceleration
α	Road slope
ρ_{air}	Air density
A_f	Vehicle frontal surface area
$\eta_{DC/DC}/\eta_{DC/AC}$	Efficiency of DC-DC/DC-AC converter
c_d	Aerodynamic coefficient
η_{mec}	Mechanical transmission efficiency
η_{EM}	Electrical machine efficiency
η_{FC}	Efficiency of fuel cell system
ρ_{H_2}	Chemical energy density of H2
m_{H_2}	H2 mass consumption
$P_{chemical}$	Theoretical power supplied by H2
P_{stack}	Fuel cell stack power
P_{AUX}	Power consumed by auxiliaries
$[P_{\eta_{lower}}, P_{\eta_{upper}}]$	High efficiency region of FCS
η_{max}	Maximum fuel cell system efficiency
η_{BAT}	Battery efficiency
I_{BAT}	Battery current
Q_{BAT}	Battery nominal capacity
V_{OC}	Open-circuit voltage
R_{BAT}	Battery internal resistance
V_{DC}	DC bus voltage
ω_{motor}	Motor rotational speed
T_{motor}	Motor torque
η_{motor}	Motor efficiency
V^*	Forecasted speed profile
T_{trip}	Estimated trip duration
$(.)_{ref}$	Reference value
U_{opt}	Optimal control policy
N_c	Number of cluster centers
$C = \{c_1, \ldots, c_{N_c}\}$	Fuzzy cluster centers
$U \in R^{n \times N_c}$	Fuzzy partition matrix
μ_{ij}	Fuzzy membership degree
$[T_l]_{ij}$	Transition probability
ΔT	Sampling period
r_{soc}/r'_{soc}	Reference/adjusted SoC depleting rate
$\rho(k)$	Adjusting factor
J_k	k-th MPC cost function
C_1, C_2, C_3	MPC cost terms
H_m	Speed sample length
ΔP_{FC}	Fuel cell power transients
$x = [\mathrm{V_{ave}}, \mathrm{V_{std}}, \mathrm{A_{ave}}]$	Normalized feature vector
$\omega_1, \omega_2, \omega_3$	MPC penalty coefficients
k_ρ	Positive constant
H_p	Prediction horizon
SoC_{end}	Terminal SoC
$m_{H_2}^{equ}$	Equivalent H2 consumption
$\overline{\lvert\Delta P_{fc}\rvert}$	Average fuel cell power transients
T_{cal}	Calculation time per step
r_{high}	High efficiency ratio

Section I. Introduction

Nowadays, technique advancements on plug-in hybrid electric vehicles (PHEVs) have attracted substantial attentions because of its potential in reducing the emission of greenhouse gases [1]. To further mitigate the dependency on fossil fuels, the onboard proton exchange membrane fuel cell (PEMFC)

systems, which can transform the hydrogen energy into electricity power, are becoming the competitive alternative to traditional internal combustion engines (ICE). As the combination of these advanced technologies, FC-based PHEVs (FCPHEV) have become one of the research hotspots in the transportation electrification field during past few years [2].

A robust energy management strategy (EMS) is indispensable in achieving the efficient power allocation among multiple energy/power sources within the vehicles' hybrid powertrain. Among existing EMSs for conventional PHEVs, improving the fuel economy is regarded as one of the primary optimization objectives. In contrast, owing to the extremely high costs of the vehicular fuel cell systems (FCS), slowing down its performance degradations caused by improper operations (e.g. frequent on-off cycles and dynamic loading conditions [3] etc.) is another significant EMS objective [4]. Despite numerous efforts made in previous researches, how to devise a multi-objective real-time applicable EMS for FCPHEVs that can both improve fuel efficiency and prolong the FCS's lifetime still needs to be sufficiently investigated.

1.1. Literature review

Existing EMSs for hybrid electric vehicles (HEVs) can be categorized into rule-based strategies and optimization-based strategies. A rule-based strategy distributes the power demands based on the characteristic of energy sources [5]-[7] or a series of deterministic or fuzzy rules [8]-[10], where the major advantage lies in the real-time suitability. However, the EMS performance optimality cannot be fully guaranteed by the expertise knowledge or engineering experiences. In contrast, for achieving the global optimal performances, various EMSs based on dynamic programming (DP) [11], Pontryagin's minimum principle (PMP) [12], [13] and Genetic algorithm (GA) [14] are developed. However, these strategies are only served as the offline benchmarks rather than being implemented for real-time applications due to the requirement on the full trip knowledge and the associated huge computation burdens.

In this case, EMSs relying on real-time optimizations have attracted substantial research interests, like Equivalent Consumption Minimization Strategy (ECMS) [15], Extremum Seeking Method [16] and Model Predictive Control (MPC) [17]-[19]. For instance, benefiting from the sequential quadratic programming (SQP) technique, the optimal power splitting decisions from the presented ECMS are

obtained by taking into account the dynamic behaviors of three power sources [15]. It has been verified experimentally that the proposed EMS can improve fuel economy by at least 2.16% compared to a benchmark rule-based EMS. As a compromise between the instantaneous optimization (e.g. ECMS) and the global optimization (e.g. DP) [20], MPC can generate control sequences by taking into account the upcoming state trajectories within the finite time horizon. Specifically, owing to the usage of short-term (e.g. 1 to 10s) predictive speed traces, the MPC strategy has achieved 7% fuel consumption conservation against a simple ECMS strategy [21]. Therefore, considering its strong ability in handling future uncertainties [22], this paper employs the MPC framework for developing the predictive EMS (PEMS).

To enhance the MPC control performance, a reliable speed forecasting method should be devised. Actually, plenty of attempts were made on this topic, where the Markov Chain (MC) based stochastic models [23]-[25] and the neural network (NN) based machine learning approaches [26]-[28] become two representative techniques. For example, a multi-step MC model is employed for speed forecasting over each rolling optimization horizon [23]. Besides, a deep NN velocity predictor established in [26] can reduce the average prediction error by 22.39% compared to a back propagation NN predictor (BPNN). Although various speed-forecasting approaches have been successfully developed, there still exhibits plenty room for improvement regarding the prediction accuracy. Actually, drivers' intentions would change accordingly with the vehicles' operation states [29]. For example, aggressive driving behaviors with large acceleration would be detected in the vehicles' start-up phases, while mild driving behaviors tend to appear during the vehicles' cruising phases. Apparently, various driving intentions would lead to the significantly different future velocity distributions. Hence, if a single-mode predictive model were used to cope with multiple types of input driving states, the overall reliability of velocity prediction would be compromised [30], which is a common drawback for conventional speed forecasting approaches. Therefore, a multi-mode velocity predictor for adapting to various driving conditions deserves further investigations.

Additionally, for guiding the future battery energy usage of PHEVs, the state-of-charge (SoC) reference generation methodologies should be properly devised. Given the trip length (or duration), authors in [23], [31] use linear SoC reference model to plan battery energy depletion. Moreover, based on the traffic

information from global positioning systems (GPS) and intelligent transportation systems (ITS), SoC reference traces can be extracted by global optima searching algorithms [20], [32]. For example, in a hierarchical EMS [20], DP is performed on the traffic flow speed for obtaining the optimal SoC trajectories. Afterwards, the reference SoC values are inserted into the MPC tracking controller. In this case, the proposed EMS can achieve nearly 95% fuel optimality as DP basis. Besides, data-driven approaches also show the effectiveness in generating SoC reference [33], [34]. For example, in [34], multiple DP-optimized SoC trajectories under various speed profiles are served as the training sample for a neuro-fuzzy model. The well-trained model is then employed for online SoC reference generation given the knowledge of trip length and average trip speed. Correspondingly, 4% fuel consumption saving can be realized by the presented EMS against a PMP benchmark. However, regarding previous SoC reference generation methods, the exceeding requirements on trip knowledge or the huge computation burdens greatly threaten their real-time practicality. Consequently, a time-efficient battery energy planning method with less dependency on real-time traffic information should be further studied.

1.2. Motivations and contributions

To sum up, several limitations can be found in previous researches: 1) to improve the MPC control performance, the accuracy and robustness of existing speed forecasting methods should be further enhanced. 2) When planning the battery energy usage, the dependency on the previewed traffic information needs to be reduced for enhancing the real-time suitability. 3) A multi-objective strategy considering both the fuel economy and the FCS's lifetime prolongation deserves further studies.

To bridge these research gaps, this paper presents an online power allocation strategy for a fuel cell electric vehicle designed for urban postal-delivery, containing following major contributions:

- An improved velocity predictor based on multi-step Markov Chain and fuzzy C-means clustering technique is presented, which contains multiple predictive sub-models for dealing with different input driving states. The prediction robustness is enhanced by a fusion strategy, which aggregates the forecasted speed profiles from all sub-models with the real-time quantified fuzzy membership degrees.

- With velocity prediction results and partially previewed traffic information, a computation-friendly SoC reference generator is proposed for regulating battery energy depletion rates against different driving conditions.
- A multi-criteria optimization-based EMS considering simultaneously the hydrogen utilization efficiency and the FCS durability is presented, where, at each sampling time instant, the desirable control policy is derived through repeatedly minimizing the MPC performance index.
- The results of EMS performance evaluation demonstrate (1) the increased velocity prediction precision over conventional predictors; (2) the improvement on fuel cell working efficiency and durability of the proposed EMS against benchmark strategies; (3) the proposed EMS is robust to certain level of trip duration estimation errors, indicating the practicality for real applications.

1.3. Outline

The sequel of this paper is arranged as follows. The powertrain modeling of the light-duty mail-delivery FCPHEV is given in section II. Section III presents the development of the velocity predictor, the adaptive SoC reference generator and the MPC-based EMS. In section IV, the comparative EMS performance evaluation is carried out. Section V briefs the major conclusions.

Section II. System modeling

2.1. Light-duty Vehicle Powertrain Model

The HEVs' powertrain design (e.g. the degree of hybridization, the components sizing etc.) and the development of corresponding EMSs affect each other, which thus deserves substantial attentions when devising the control strategies for HEVs, especially for the FC-based ones [35]. In this study, the EMS is designed for a light-duty mail-delivery vehicle, which is the prototype that has been built in the "Mobypost" project [36], where the essential vehicular parameters are presented in table 1. Additional details concerning the vehicle powertrain design can be found in [37].

Fig. 1(a) schematically depicts the vehicle's powertrain structure. The onboard PEMFC system is connected to the DC bus by a DC-DC converter, whereas the rechargeable battery pack is straightly plugged into the DC bus. During the vehicles' operation, the battery pack is dedicated to supplying the peaking power during the acceleration phases and to absorb a portion of negative power during the

regenerative braking phases. In contrast, the FCS aims at working steadily to charge the battery pack for extending the vehicles' driving mileage.

Given the vehicle's mass m_v and speed v, by analyzing the vehicle's dynamics in motion (Fig. 1(b)), the power request from wheel side P_{pro} is denoted by (1) [38]. Subsequently, the output power from FCS (P_{FC}) and battery pack (P_{BAT}) jointly satisfy the DC bus power request (P_d), as denoted in (2).

$$P_{pro}(t) = v(t) \cdot (m_v \frac{dv(t)}{dt} + c_r m_v g \cos(\alpha) + m_v g \sin(\alpha) + \frac{1}{2} \rho_{air} A_f c_d v(t)^2) \quad (1)$$

$$P_d(t) = \frac{P_{pro}(\mathrm{t})}{\eta_{mec} \cdot \eta_{DC/AC} \cdot \eta_{EM}} = P_{FC}(t) \cdot \eta_{DC/DC} + P_{BAT}(t) \quad (2)$$

where c_r represents the coefficient of rolling resistance, ρ_{air} the ambient air density, A_f the vehicles' front surface area, c_d the aerodynamic coefficient. In addition, η_{mec} and η_{EM} denote the efficiency of mechanical transmission and electrical machine, respectively, while $\eta_{DC/AC}$ and $\eta_{DC/DC}$ respectively denote the efficiency of DC/AC and DC/DC converters. Please note the gravitational acceleration *g* is taken as 9.81 m/s^2 and road slope α is assumed as zero in this study.

TABLE 1. Vehicular parameters regarding the powertrain model

Component	Description	Value	Data Source
Mobypost Structural Parameters	Weight	579 kg	Mobypost Vehicle Prototype [37]
	Frontal surface area	2.48 m^2	
	Density of air	1.26 kg/m^3	
	Drag coefficient	0.7	
	Rolling Resistance coefficient	0.015	
	Mechanical transmission efficiency	0.92	Assumption
PEMFC System	Peak power	1200 W	Quasistatic Fuel Cell Model [38]+ Database in [39]
	Peak Efficiency	43%	
Li-Ion Battery	Nominal Energy capacity	5.5 kWh	Mobypost Vehicle Prototype [37]
Traction Electrical Machine	Permissible max. Power	30 kW	Database in Open-Source Software ADVISOR [40]
	Permissible max. Torque	125 Nm	
	Permissible max. Speed	9000 rpm	
Uni. DC/DC converter	Constant Efficiency	0.90	Assumption
Bio. DC/AC inverter	Constant Efficiency	0.95	

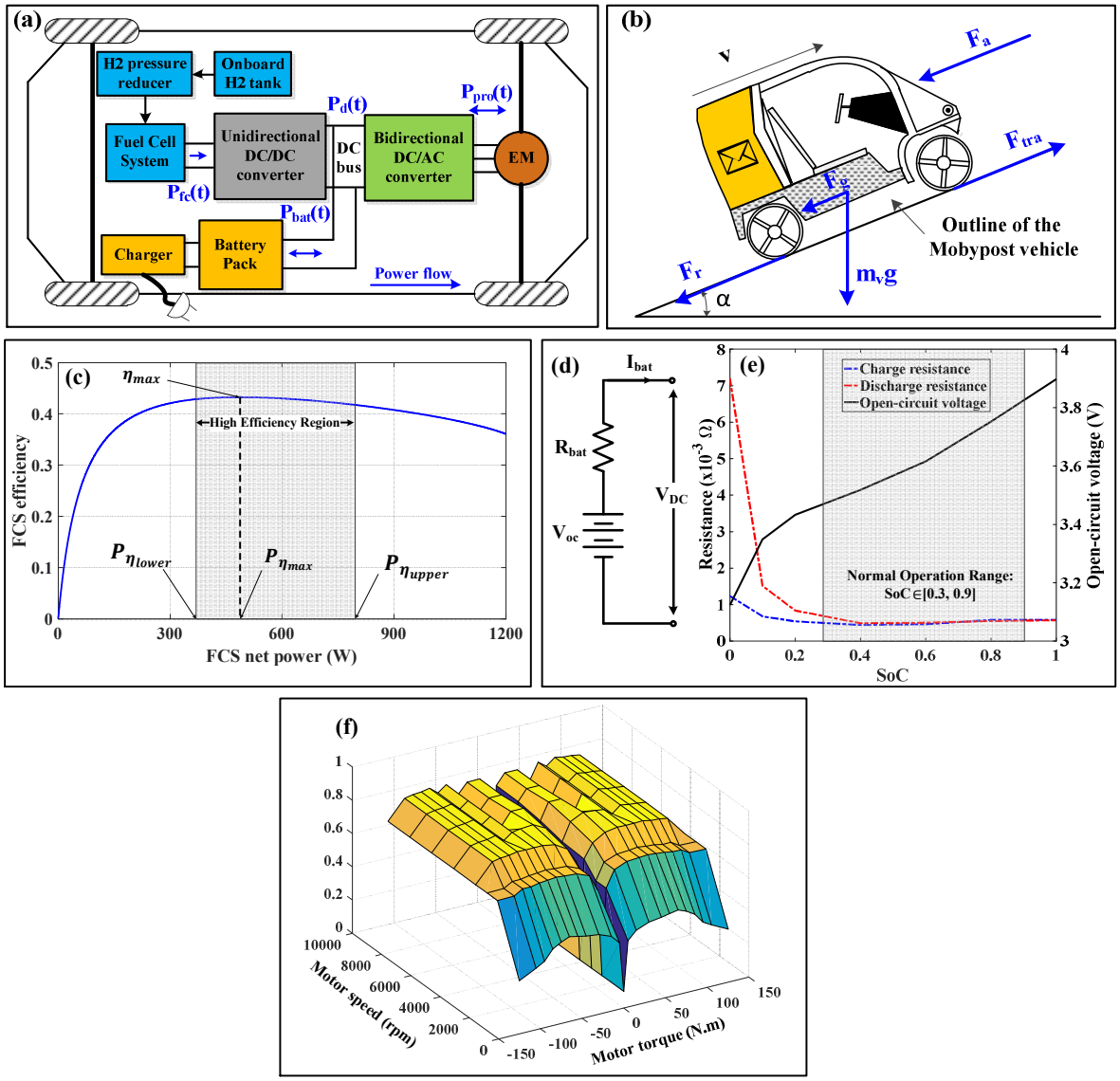

Fig. 1. Light-duty FCHEV modeling. (a) Vehicle's powertrain architecture; (b) Vehicle's dynamics in motion; (c) Onboard PEMFC system efficiency as a function of P_{FC}; (d) Battery model: equivalent circuit of R-int model; (e) Characteristics of the studied battery cell: the resistance and the OCV as a function of SoC; (f) EM working efficiency given by the 2-D look-up table (map).

2.2. Fuel Cell Model

To mitigate the vehicle's range anxiety during the postal delivery, the PEMFC system is designed to work steadily for charging the power battery pack. Additionally, given the H2 chemical energy density (ρ_{H_2} , in MJ/kg), the mass of H2 (m_{H_2}) consumed during the tasks can be computed by [9]:

$$m_{H_2} = \int_0^t \frac{P_{FC}(t)}{\eta_{FC} \cdot \rho_{H_2}} dt \tag{3}$$

where η_{FC} represents the system efficiency of PEMFC. In this work, a quasistatic fuel cell model is employed, where the polarization curve of a single fuel cell is given under specific operation conditions (e.g. humidity, temperature etc.) [38]. Furthermore, within the PEMFC system, given the gross power produced by the fuel cell stack (P_{Stack}), the power consumed by all auxiliary components (P_{AUX}) and the theoretical power supplied by H2 ($P_{Chemical}$), η_{FC} can be defined as [41]:

$$\eta_{FC} = \frac{P_{Stack} - P_{AUX}}{P_{Chemical}} = \frac{P_{FC}}{P_{Chemical}} \tag{4}$$

where P_{FC} reflects the effective portion of fuel cell system power that can be delivered to the external (net power) [41]. The studied PEMFC system efficiency as a function of P_{FC} is specified in Fig. 1(c). Note the peak efficiency (η_{max}) corresponds to the most efficient operating point of the PEMFC system, marked as $P_{\eta_{max}}$. Besides, let $[P_{\eta_{lower}}, P_{\eta_{upper}}]$ represents the high efficiency area of the PEMFC system, where $P_{\eta_{lower}}$ and $P_{\eta_{upper}}$ are respectively set to 1/3 and 2/3 of its peak power (1.2 kW) [9].

2.3. Battery Model

The R-int model is employed to represent the power battery pack, whose equivalent circuit is displayed in Fig. 1(d). Moreover, given the battery current (I_{BAT}), the internal resistance (R_{BAT}), the open-circuit voltage (OCV, marked as V_{OC}), the nominal capacity (Q_{BAT}) and the battery efficiency (η_{BAT}), the voltage on DC bus (V_{DC}) is calculated by (5).

$$\frac{dSoC(\mathrm{t})}{dt} = -\frac{\eta_{BAT} \cdot I_{BAT}(\mathrm{t})}{Q_{BAT}} \tag{5a}$$

$$I_{BAT}(\mathrm{t}) = \frac{\mathrm{V}_{OC}(\mathrm{SoC}) - \sqrt{\mathrm{V}_{OC}(\mathrm{SoC})^2 - 4R_{BAT}(\mathrm{SoC})P_{BAT}(\mathrm{t})}}{2R_{BAT}(\mathrm{SoC})} \tag{5b}$$

$$V_{DC} = V_{OC}(SoC) - I_{BAT} \cdot R_{BAT}(SoC) \tag{5c}$$

where SoC is a percentage indicator (0 to 1) of the residual battery capacity. Furthermore, as indicated in Fig. 1(e), the numerical values of battery parameters (e.g. the OCV and the resistance) vary according to

battery SoC. Note the feature of the studied battery cell (6Ah Lithium-ion battery module) is extracted from ADVISOR [40]. To ensure the normal operation of battery pack, it is expected to maintain SoC within the range [0.3, 0.9] [24].

2.4. Electrical Machine Model

Thanks to the abundant Electrical Machine (EM) models from ADVISOR, an AC asynchronous motor is picked in this work, whose output power peaks at 30 kilowatt. Besides, the physical limitations of the EM speed (ω_{motor}) and torque (T_{motor}) are [0, 9000] rpm and [-125, 125] N·m, respectively. Moreover, the EM efficiency (η_{motor}) is determined by its working state specified by ω_{motor} and T_{motor} . Such relationship can be denoted as $\eta_{motor} = q(\omega_{motor}, T_{motor})$, which is typically given in the form of discrete 2-D look-up table. Hence, once the speed and torque requests are specified, η_{motor} is derived through the look-up table extracted from ADVISOR (Fig. 1(f)).

Section III. Development of predictive energy management strategy

The system-level block diagram of the presented hierarchical PEMS is depicted in Fig. 2. In supervisory level, the upcoming speed profile (V^*) is generated by the velocity predictor. Subsequently, with the estimated trip duration (T_{trip}), the SoC reference (SoC_{ref}) is generated for planning the battery energy usage. Combined with the velocity prediction results and SoC reference, the MPC controller generates the control policies (U_{opt}) by minimizing the multi-objective cost function within each rolling optimization horizon, where the sampling period ΔT is set to 1s.

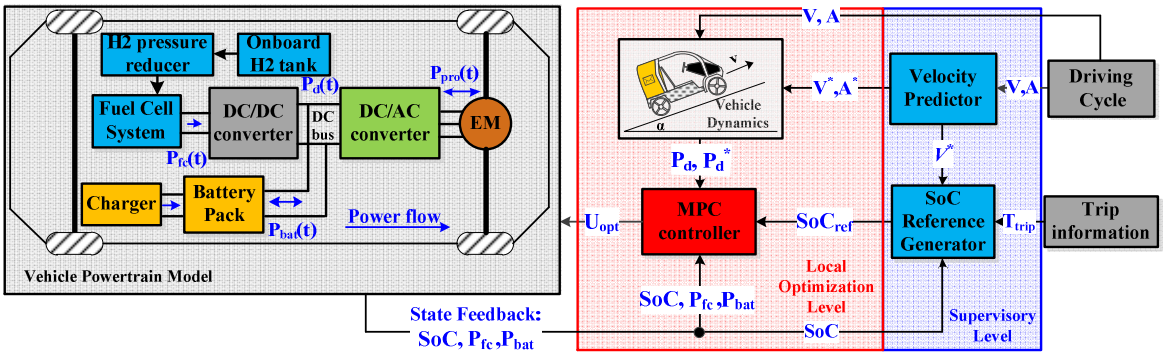

Fig. 2. Schematic diagram of the proposed PEMS.

3.1. Improved Markov Chain Velocity Predictor

To guarantee the MPC control performance, a reliable speed-forecasting methodology should be developed. Under realistic driving conditions, drivers' intentions would vary from vehicles' operation stages, leading to different distributions of future velocity. Therefore, if a single-mode prediction model were used to characterize the future velocity distributions under multiple vehicle operation stages, the overall prediction performance would be compromised. To address this issue, a velocity predictor based on fuzzy C-means clustering and multi-step Markov Chain (FCM-MC) is proposed. Specifically, the FCM is used to capture the feature of recent driving states and the final prediction results are obtained by synthesizing the forecasted speed profiles from all MC sub-models with the quantified fuzzy membership degrees. The detailed design process will be presented subsequently.

3.1.1. Fuzzy classification and Markov predictive model estimation

As shown in Fig. 3, the proposed speed forecasting method includes two working phases. This subsection presents the principal of offline working phase.

- **Driving data pre-processing by fuzzy C-means clustering technique**

To establish multiple predictive sub-models, the original driving database should be classified into several groups based on the feature of driving samples. In this study, the driving profiles for building the MC prediction models are extracted from the GPS-collected database on the mail delivery routes, which contains the speed and acceleration sequences, namely $[v_1, \dots, v_N]$ and $[a_1, \dots, a_N]$. Afterwards, the original driving database is partitioned into numerous H_m- dimensional driving vectors, where the *k*-th sample can be expressed as $[v_{\mathrm{k}}, \dots, v_{\mathrm{k+H_m-1}}]$ and $[a_{\mathrm{k}}, \dots, a_{\mathrm{k+H_m-1}}]$. Furthermore, three parameters are selected to characterize each driving sample, namely the average speed v_{k_ave}, the speed standard deviation v_{k_std} and the average acceleration a_{k_ave}. To eliminate the negative impacts on classification results by different data scales, the k-th feature vector $x_k = [\mathrm{V_{k\_ave}}, \mathrm{V_{k\_std}}, \mathrm{A_{k\_ave}}]$ is composed of the corresponding normalized terms, where $\mathrm{V_{k\_ave}} = \frac{v_{k\_ave}}{v_{ave}^{max}} \in [0,1], \mathrm{V_{k\_std}} = \frac{v_{k\_std}}{v_{std}^{max}} \in [0,1], \mathrm{A_{k\_ave}} = \frac{a_{k\_ave} - a_{ave}^{min}}{a_{ave}^{max} - a_{ave}^{min}} \in [0,1]$. Besides, the superscripts "max" and "min" specify the extremum of corresponding physical quantities. Therefore, each driving sample is denoted by a three-dimensional feature vector x.

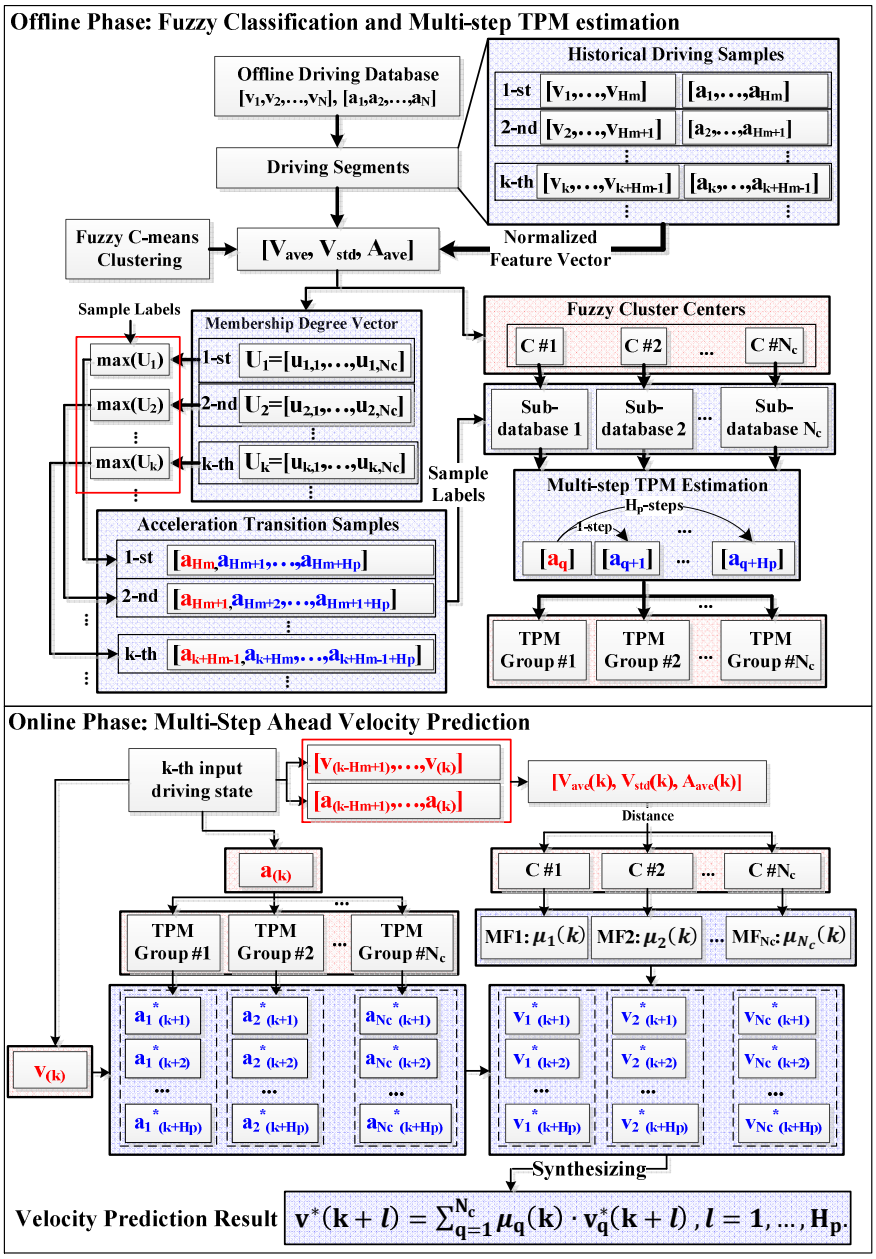

Fig. 3. Working Flow of the speed forecasting method using Markov Chain and Fuzzy C-means clustering.

As there is no uniform definition on the pattern of driving state x, the classification process should be unsupervised. To perform the unsupervised classification, the FCM technique is introduced. Given the number of clusters N_c and a finite dataset $X = \{x_1, \dots, x_n\}$, the FCM returns a list of cluster centers $C = \{c_1, \dots, c_{Nc}\}$ and a fuzzy partition matrix $U \in R^{n \times N_c}$, where its (i, j)-th element $\mu_{ij} \in [0,1]$ $(i = 1,2, \dots, n, j = 1,2, \dots, N_c)$ indicates the membership degree of the data point x_i in the j-th cluster. The sum of membership value in all clusters equals to one, namely $\sum_{j=1}^{N_c} \mu_{ij} = 1$. The FCM working process is summarized in table 2 [42].

TABLE 2. Working process of the FCM method.

Step	Content
1	Randomly initialize all cluster membership values $\mu_{ij}, i \in \{1, \dots, n\}, j \in \{1, \dots, N_c\}$.
2	Calculate the centroid by $c_j = \frac{\sum_{i=1}^{n} \mu_{i,j}^{m} \cdot x_i}{\sum_{i=1}^{n} \mu_{i,j}^{m}}$, where the parameter m $(m > 1)$ is fuzzy partition matrix exponent, which is used to control the degree of fuzzy cluster overlap. A larger m means a higher degree of fuzziness in neighboring clusters.
3	Update μ_{ij} by $\mu_{ij} = \frac{1}{\sum_{k=1}^{N_c} \left(\frac{\|x_i - c_j\|}{\|x_i - c_k\|} \right)^{\frac{2}{m-1}}}$, where the operator $\|\cdot\|$ means the Euclidean Distance from the data point x_i to centroid c_j.
4	Calculate the value of $J_m = \sum_{i=1}^{n} \sum_{j=1}^{N_c} \mu_{ij}^{m} \|x_i - c_j\|^2$.
5	Repeat step 2 to 4 until J_m decreases by smaller than the predefined limit or other termination conditions are satisfied (e.g. maximum iteration number reached etc.).

To obtain the deterministic classification results, the largest membership degree μ_{i_max}, where $\mu_{i\_max} = \max[\mu_{i1}, \dots, \mu_{iN_c}]$, labels the feature vector x_i to one of N_c clusters. Based on the labels, corresponding acceleration transition database (where the k-th sample is marked as $[a_{\mathbf{k+H_m-1}}, \dots, a_{\mathbf{k+H_m-1+H_p}}]$) is divided into N_c sub-databases, where H_p is prediction horizon. The acceleration samples within each sub-database are then used to estimate the multi-step transition probability matrices (TPM) of the corresponding MC predictive sub-model.

- **Multi-step TPM Estimation**

MC is used to characterize the future probability distribution of acceleration. Based on the interval encoding method [43], the continuous acceleration domain is separated into a finite set of disjoint intervals, $I_j, j \in \{1, \dots, s\}$. Each interval is associated with a MC state, $a_j \in I_j$, which is the midpoint of interval I_j. Besides, let a countable set $\{a_1, \dots, a_s\}$, which contains all possible acceleration states, denotes the MC state-space. In this case, the future acceleration distribution in multi-step ahead is described by a TPM group $T_G = \{T_1, \dots, T_{H_p}\}$, where each TPM is an s-by-s matrix. Within the $l\text{-}th$ TPM in T_G, the element located in the $i\text{-}th$ row and $j\text{-}th$ column (marked as $[T_l]_{ij}$) represents the probability of a MC state transition incident, which begins at a_i and terminates at a_j in l-steps ahead. Hence, $[T_l]_{ij}$ is calculated based on the maximum likelihood estimation approach.

$$[T_l]_{ij} = \Pr\{a(k+l) = a_j \,|\, a(k) = a_i\} \approx N_{ij}^{l} / N_i^{l}, l \in \{1, \dots, H_p\}, i, j \in \{1, \dots, s\}. \quad (6)$$

N_{ij}^{l} and N_{i}^{l} represent the MC state transition times, where the superscript l indicates the transition time step. The subscripts specify the starting and ending index of the state transition incidents, where ij means the transition is from state i to state j, while i means the transition is originating from state i. Note the TPM group T_G is estimated based on the samples within one of N_c sub-databases. Similarly, with all sub-databases, N_c TPM groups $\{T_{G\_1}, \dots, T_{G\_N_c}\}$ can be established based on (6).

3.1.2. Real-time fuzzy membership degree quantification and multi-step velocity prediction

Once the cluster centers $\{c_1, \dots, c_{N_c}\}$ and N_c TPM groups $\{T_{G\_1}, \dots, T_{G\_N_c}\}$ are established, they can be used for multi-step speed forecasting. Three working steps of velocity prediction are given as follows:

- At $t = k$, sample the k-th driving states, namely $[v(k + \mathrm{H_m} - 1), \dots, v(k)]$ and $[a(k + \mathrm{H_m} - 1), \dots, a(k)]$, and calculate the corresponding normalized feature vector, namely $x(k) = [\mathrm{V_{ave}}(k), \mathrm{V_{std}}(k), \mathrm{A_{ave}}(k)]$. Afterwards, quantify the membership degree of $x(k)$ in N_c clusters, where the quantification result is expressed by $[\mu_1(k), \dots, \mu_{N_c}(k)]$.
- Encode the acceleration $a(k)$ into the MC state a_i. Then, the l-step ahead acceleration is computed by the mathematical expectation, according to the interval midpoints: $a_q^*(k + l) = \sum_{j=1}^{s} [T_l^q]_{ij} \cdot a_j \,, if\ a(k) \in I_i$, where $T_l^q \in T_{G\_q}, q = 1, \dots, N_c, l = 1, \dots, H_p$. Afterwards, the velocity prediction result from the q-th MC sub-model is expressed by: $v_q^*(k + l) = v(k) + \sum_{r=1}^{r=l} a_q^*(k + r) \cdot \Delta T$.
- By synthesizing the quantified membership degree with the velocity prediction results from all MC sub-models, the final speed forecasting result is: $v^*(k + l) = \sum_{q=1}^{N_c} \mu_q(k) \cdot v_q^*(k + l)\,, l = 1, \dots, H_p$. Finally, the polynomial fitting algorithm is employed to smooth the forecasted speed profiles.

It should be mentioned that, by using the weighted velocity prediction results from all MC sub-models, it is beneficial to reduce the negative impacts on prediction reliability caused by the identification uncertainty of the input driving states.

3.2. Adaptive Battery SoC Reference Generator

The plug-in technology allows the energy stored in the onboard battery pack to be depleted during the mail-delivery tasks. For scheduling the battery energy usage, the SoC reference is indispensable within

each rolling optimization horizon. By tracking the given SoC reference, the EMS controller can manipulate the battery output power with respect to the rapid-changing external power demands. Considering the changeable traffic conditions during mail delivery tasks, the vehicle would operate under different modes, meaning different types of power demand could be detected. In fact, two typical driving conditions could be found within vehicles' actual speed profiles, namely the flowing (Fig. 4(a)) and congested driving conditions (Fig. 4(b)), respectively.

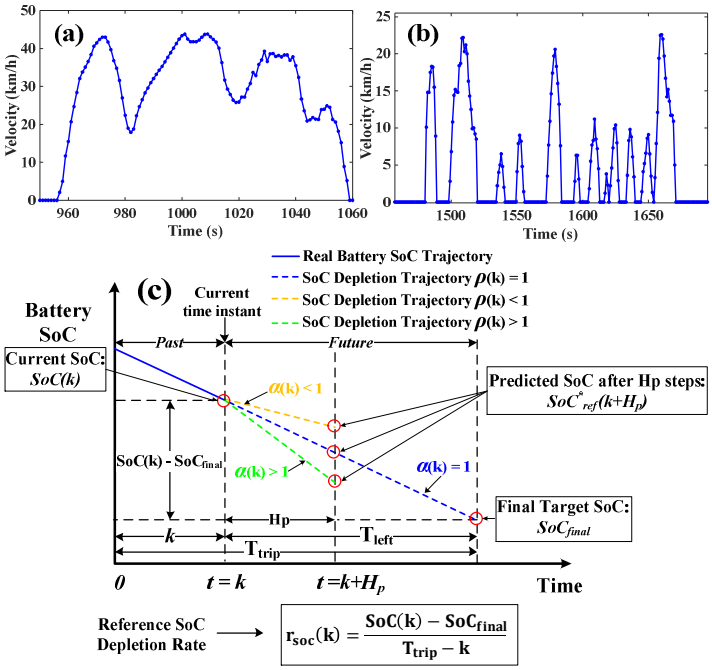

Fig. 4. (a) Flowing and (b) congested driving conditions of Mobypost vehicle. (c) Working principle of the SoC reference generator.

Under flowing driving conditions, the vehicles' speed changes mildly and the average is relatively high, indicating the higher average power demand. In contrast, frequent vehicle stops can be found under congested driving conditions, where the vehicles' speed changes sharply and the average is relatively low. Therefore, lower average power demand could be detected in this case. To regulate the SoC depleting rate towards different driving conditions, an adaptive SoC reference generator is proposed, whose working principle is illustrated in Fig. 4(c).

Since the mail-delivery tasks are conducted on the relatively fixed routes, it is assumed that the trip duration can be estimated before departure. At $t = k$, given the current SoC, the final target SoC and the velocity prediction results $\mathrm{V}_k^* = [v^*(k+1), ..., v^*(k+\mathrm{H_p})]$, the forecasted SoC reference after $\mathrm{H_p}$ steps can be calculated by:

$$SoC_{ref}^{*}(k+\mathrm{H_p}) = SoC(k) - \boldsymbol{r}_{soc}^{'} \cdot \mathrm{H_p} \tag{7a}$$

$$\boldsymbol{r}_{soc}^{'}(k) = \rho(k) \cdot \boldsymbol{r}_{soc}(k) = \rho(k) \cdot \frac{SoC(k) - \mathrm{SoC}_{final}}{T_{trip} - k} \tag{7b}$$

$$\rho(\mathrm{k}) = \frac{k_{\rho}}{1 + \frac{v_{std}^{*}(k)}{v_{mean}^{*}(k)}} \tag{7c}$$

where $r_{soc}(k) = \frac{SoC(k) - SoC_{final}}{\mathrm{T}_{trip} - k}$ is the average SoC depleting rate against the remaining trip duration, which is taken as the reference depletion rate at $t = k$. In addition, r'_{soc} is the adjusted SoC depletion rate and ρ is the adjusting factor, where the positive constant k_{ρ} defines the upper limit of ρ. A small k_{ρ} would reduce the overall SoC depletion rate, making the battery energy not fully utilized, while an overlarge k_{ρ} would deplete the battery energy too fast, leading to the extended charge-sustaining (CS) driving phases. Therefore, a proper k_{ρ} should be used to seek a balance between the battery utilization rate and the overall EMS performance.

Furthermore, $v^{*}_{mean}(k)$ and $v^{*}_{std}(k)$ respectively denote the average and standard deviation of the forecasted speed V_k^{*}. It should be mentioned that a larger v^{*}_{mean} and a smaller v^{*}_{std} imply the flowing driving conditions, leading to a larger ρ. On the contrary, a smaller v^{*}_{mean} and a larger v^{*}_{std} indicate the congested driving conditions, thus resulting in a smaller ρ. Hence, the actual SoC depletion rate r'_{soc} can be regulated by ρ. When $\rho > 1$, the actual SoC depletion rate r'_{soc} is higher than the reference rate r_{soc}. When $\rho < 1$, the actual SoC depletion rate r'_{soc} is lower than r_{soc}. Specially, $\rho = 0$ when and only when $v^{*}_{mean} = 0$.

Besides, to prevent battery over-charge or over-discharge, $\mathrm{SoC}^{*}_{\mathrm{ref}}$ is restricted within the allowable boundaries, namely $\mathrm{SoC}^{*}_{\mathrm{ref}} \in [SoC_{min}, SoC_{max}]$, where SoC_{min} and SoC_{max} are respectively set as 0.3 and 0.9. Please note that $[SoC_{min}, SOC_{max}]$ only defines the range of SoC reference value. If the actual SoC escapes from this range, the EMS emergency mode would be activated to force SoC back to [0.3, 0.9] as soon as possible.

3.3. Model Predictive Controller

MPC takes advantages of the estimated system future behaviors for decision-making, which is especially suitable for controlling the complex systems with multiple variables and constraints (e.g. the HEVs' powertrain systems). The proposed MPC is thoroughly introduced in subsection 3.3.

3.3.1. Control-oriented model

Considering the limited resources of the onboard electronic control units, a linear-quadratic MPC model (with $\Delta T = 1s$) is adopted. Specifically, given the state vector $\boldsymbol{x} \in R^{2\times1}$, the manipulated variable $\boldsymbol{u} \in R^{1\times1}$, the output vector $\boldsymbol{y} \in R^{2\times1}$, the reference $\boldsymbol{r} \in R^{2\times1}$ and the disturbance $\boldsymbol{w} \in R^{1\times1}$ of the studied system, the control-oriented model can be defined by (8).

$$\begin{aligned}
&\boldsymbol{x}(k+1) = \mathbf{A}(k)\boldsymbol{x}(k) + \mathbf{B}_{\mathrm{u}}(k)\boldsymbol{u}(k) + \mathbf{B}_{\mathrm{w}}(k)\boldsymbol{w}(k)\\
&\boldsymbol{y}(k) = \mathbf{C}\boldsymbol{x}(k) + \mathbf{D}\boldsymbol{u}(k)\\
&\begin{cases}
\boldsymbol{x}(k) &= [\mathrm{SoC}(k), P_{\mathrm{FC}}(k-1)]^{\mathrm{T}}\\
\boldsymbol{u}(k) &= \Delta P_{\mathrm{FC}}(k) = \dfrac{P_{\mathrm{FC}}(k) - P_{\mathrm{FC}}(k-1)}{\Delta T}\\
\boldsymbol{y}(k) &= [\mathrm{SoC}(k), P_{\mathrm{FC}}(k)]^{\mathrm{T}}\\
\boldsymbol{w}(k) &= P_{\mathrm{d}}(k)\\
\boldsymbol{r}(k) &= [\mathrm{SoC}_{ref}, P_{\mathrm{FC}_{ref}}]^{\mathrm{T}}
\end{cases}
\end{aligned} \tag{8}$$

Moreover, the DC power balance relationship can be denoted as the following discrete form:

$$P_d(k) = P_{\mathrm{FC}}(k)\cdot\eta_{\mathrm{DC/DC}} + P_{\mathrm{BAT}}(k) \tag{9}$$

Furthermore, the battery SoC dynamics is modeled by a first-order differential equation:

$$SoC(k+1) = SoC(k) - \frac{\Delta T\cdot\eta_{\mathrm{BAT}}}{V_{\mathrm{DC}}(\mathrm{k})\cdot\mathrm{Q}_{\mathrm{BAT}}}\cdot P_{\mathrm{BAT}}(k) \tag{10}$$

By collecting (8)-(10), the studied system matrices are given as:

$$\begin{aligned}
&\mathrm{A(k)} = \begin{bmatrix} 1 & \dfrac{\Delta T\cdot\eta_{\mathrm{BAT}}\cdot\eta_{DC/DC}}{V_{\mathrm{DC}}(\mathrm{k})\cdot\mathrm{Q}_{\mathrm{BAT}}} \\ 0 & 1 \end{bmatrix} \qquad \mathrm{B_u(k)} = \begin{bmatrix} \dfrac{\Delta T\cdot\eta_{\mathrm{BAT}}\cdot\eta_{DC/DC}}{V_{\mathrm{DC}}(\mathrm{k})\cdot\mathrm{Q}_{\mathrm{BAT}}} & 1 \end{bmatrix}^{\mathrm{T}}\\
&\mathrm{B_w(k)} = \begin{bmatrix} -\dfrac{\Delta T\cdot\eta_{\mathrm{BAT}}\cdot\eta_{DC/DC}}{V_{\mathrm{DC}}(\mathrm{k})\cdot\mathrm{Q}_{\mathrm{BAT}}} & 0 \end{bmatrix}^{\mathrm{T}} \quad \mathrm{C} = \begin{bmatrix} 1 & 0 \\ 0 & 1 \end{bmatrix} \quad \mathrm{D} = \begin{bmatrix} 0 & 1 \end{bmatrix}^{\mathrm{T}}
\end{aligned} \tag{11}$$

3.3.2. Formulation of multi-criteria objective function and constraints

Fuel efficiency and FCS lifetime expansion are two major optimization objectives. Meanwhile, the MPC controller should be able to track the battery SoC reference. Besides, the identical lengths for both MPC control and preview horizon are adopted in this work. Consequently, within the k-th rolling optimization horizon, the desirable control sequence $\mathrm{U}^{*}(\mathrm{k})=[u_{1}^{*}(\mathrm{k}),...,u_{\mathrm{H_p}}^{*}(\mathrm{k})]$ is derived through minimizing (12) with regard to (13).

$$\mathrm{J}_{k}=\sum_{i=1}^{\mathrm{H_p}}[\omega_{1}\cdot\underbrace{(\frac{\mathrm{P_{FC}}(k+i)-\mathrm{P_{FC_{ref}}}}{\mathrm{P_{FC_{max}}}})^{2}}_{\mathrm{C_1}}+\omega_{2}\cdot\underbrace{(\frac{\Delta\mathrm{P_{FC}}(k+i-1)}{\Delta\mathrm{P_{FC_{max}}}})^{2}}_{\mathrm{C_2}}]+\omega_{3}\cdot\underbrace{(\frac{\mathrm{SoC}(k+\mathrm{H_p})-\mathrm{SoC_{ref}}}{\mathrm{SoC_{max}}-\mathrm{SoC_{min}}})^{2}}_{\mathrm{C_3}} \quad (12)$$

$$\begin{cases}\underline{\mathrm{SoC}}\le\mathrm{SoC}(k+i)\le\overline{\mathrm{SoC}} & \text{(a)}\\ \underline{\mathrm{P_{FC}}}\le\mathrm{P_{FC}}(k+i)\le\overline{\mathrm{P_{FC}}} & \text{(b)}\\ \underline{\Delta\mathrm{P_{FC}}}\le\Delta\mathrm{P_{FC}}(k+i-1)\le\overline{\Delta\mathrm{P_{FC}}} & \text{(c)}\\ \underline{\mathrm{P_{BAT}}}\le\mathrm{P_{BAT}}(k+i)\le\overline{\mathrm{P_{BAT}}} & \text{(d)}\\ \boldsymbol{w}(\mathrm{k+i})=\mathrm{P}_{d}^{*}(k+i),i\ge1 & \text{(e)}\end{cases} \quad (13)$$

where $P_{FC_{max}}=1200\,W$, $\Delta P_{FC_{max}}=40\,W/s$, $SoC_{max}=0.9$, $SoC_{min}=0.3$. Three constant penalty coefficients $\omega_1,\omega_2,\omega_3$ are adjusted manually with the assistance of the global optimal EMS performance extracted by DP. As a result, $\omega_1,\omega_2,\omega_3$ are respectively set to 1, 30 and 80000 in this study. In addition, the functions of $\mathrm{C_1},\mathrm{C_2},\mathrm{C_3}$ are given as follows:

- $\mathrm{C_1}$ enforces FC operating towards the preset reference point, where the selection of $P_{FC_{ref}}$ will be introduced in section 4.2.1.
- As reported in [4], restricting FC power transients $\Delta\mathrm{P_{FC}}$ is favorable to extending the lifetime of fuel cell systems. Hence, $\mathrm{C_2}$ enables a punishment on the large FC power spikes to decelerate the FCS performance degradations owing to frequent load changes.
- $\mathrm{C_3}$ is adopted to narrow the discrepancy between the actual and reference SoC, where SoC_{ref} is provided by the SoC reference generator, namely $SoC_{ref}=SoC_{ref}^{*}(k+H_p)$. By setting C_3 as a terminal cost term, there will be additional room for MPC controller to suppress the FC power spikes owing to speed mis-predictions.

Considering the battery operation safety, (13a) defines the permissible SoC variation range, where $\underline{SoC} = 0.25$, $\overline{SoC} = 0.95$ [18]. If SoC emergency event ($SoC > 0.9$ or $SoC < 0.3$) occurs, ω_1, ω_2 are set to zero and thus the cost term C_3 could force SoC back to the normal operation range [0.3, 0.9] [18]. Moreover, due to the physical limitations, (13b)-(13d) specify the operation boundaries for both energy sources, where $\underline{P_{FC}} = 0\ W$, $\overline{P_{FC}} = 1.2\ kW$, $\underline{\Delta P_{FC}} = -\overline{\Delta P_{FC}} = 40\ W/s$, $\underline{P_{BAT}} = -10\ kW$, $\overline{P_{BAT}} = 30\ kW$. Constraint (13e) specifies the k-th measurable disturbance sequence W_k^* as $[\mathrm{P}_d^*(k+1),...,\mathrm{P}_d^*(k+\mathrm{H_p})]$. It should be mentioned that, given the k-th velocity prediction result V_k^*, P_d^* could be calculated according to (1) and (2). Furthermore, given the penalty matrices $\boldsymbol{Q}$ and $\boldsymbol{R}$, the cost function (12) can be rewritten as (14).

$$\begin{aligned} &\mathrm{J}_k^{'} = \sum_{i=1}^{\mathrm{H_p}} \left[\Delta \boldsymbol{y}(k+i)^{\mathrm{T}} \boldsymbol{Q}(k+i) \Delta \boldsymbol{y}(k+i) + \boldsymbol{u}(k+i-1)^{\mathrm{T}} \boldsymbol{R}(k+i-1) \boldsymbol{u}(k+i-1) \right] \\ &with \quad \Delta \boldsymbol{y}(k+i) = \boldsymbol{y}(k+i) - \boldsymbol{r}(k+i) \end{aligned} \tag{14}$$

In this case, by minimizing (14) subject to constraints (13), the k-th control action can be obtained, where such a quadratic programming problem is solved by the *quadprog* function embedded in the Matlab Optimization Toolbox.

Section IV. Results and Discussions

The control performance validation of the presented PEMS is carried out in the sequel of section IV.

4.1. Velocity prediction performance evaluation

Firstly, the performance of FCM-MC predictor is evaluated, where the root-mean-square-error (RMSE) is used as the criterion for prediction precision. The RMSE in the k-th prediction horizon is computed by (15a), while the average RMSE along the given cycle is given by (15b):

$$\begin{cases} RMSE(k) = \sqrt{\frac{1}{H_p} \sum_{q=1}^{q=H_p} \left(v^*(k+q) - v(k+q) \right)^2} & (a) \\ \overline{RMSE} = \frac{1}{N_{cycle}} \sum_{k=1}^{k=N_{cycle}} RMSE(k) & (b) \end{cases} \tag{15}$$

where N_{cycle} denotes the cycle duration.

4.1.1. Driving database preprocessing

As depicted in Fig. 5(a), the speed profiles of 12 mail-delivery tasks collected on the fixed routes (data sampled at 1Hz) are regarded as the original driving database for building the velocity predictor. The mileage of a single delivery task is around 25 km, which is equivalent to 4 to 4.5 hours' trip duration and the peak speed is below 60 km/h [37]. Moreover, two typical driving scenarios (flowing and congested) of the Mobypost vehicle on speed profile No.1 are given in the bottom subfigures to display the feature of mail-delivery mission profiles.

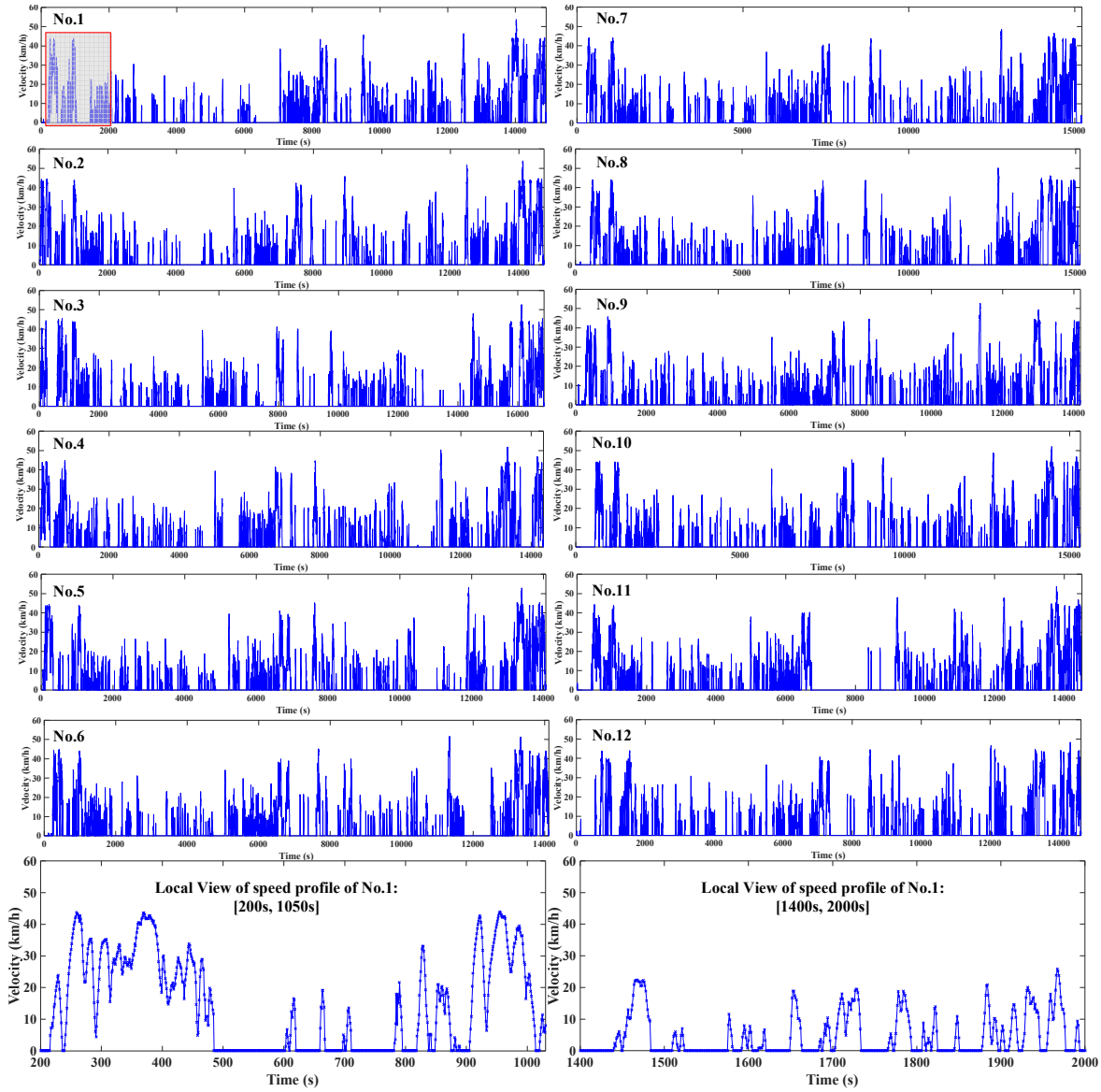

Fig. 5(a). Actual speed profiles collected by GPS on the mail-delivery routes.

Before TPM estimation, this database should be divided into N_c sub-databases according to the feature of driving samples. Taken $\mathrm{H_m} = 5$ as an example, the FCM is performed on all $\mathrm{H_m}$ – dimensional driving

samples (speed vector) extracted from the original database. The deterministic clustering results are derived by the largest element within the quantified membership degree vector, as depicted in Fig. 5(b)-(d). As can be seen, by labeling the original driving samples with the feature vector $[V_{ave}, V_{std}, A_{ave}]$, the driving database are categorized into N_c groups, where the speed samples in each group are associated with similar changing tendencies (e.g. upwards, downwards, cruising etc.). In addition, using a larger N_c makes the samples within each cluster distributed closer to each other, meaning the stronger correlation. However, the sample discrepancies among different sub-groups are insignificant if an overlarge N_c is used (e.g. samples in cluster 7 and 8 of Fig. 5(d)), implying the risk of over-classification.

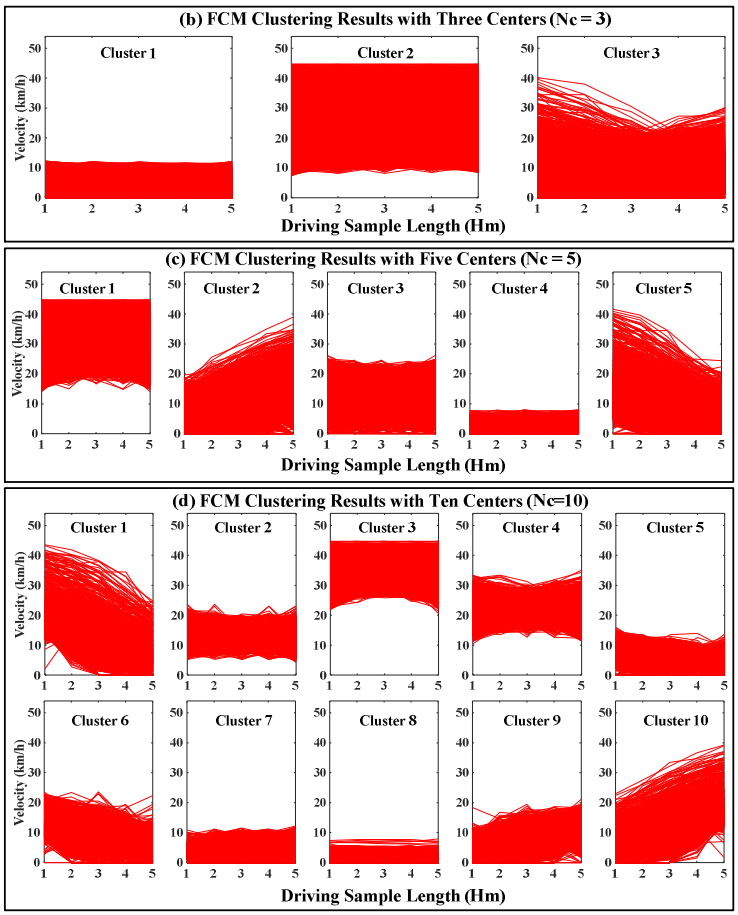

Fig. 5(b)-(d). FCM clustering results (Driving sample length: $H_m = 5$) with different N_c: (b) $N_c = 3$, (c) $N_c = 5$ and (d) $N_c = 10$.

Furthermore, the length of driving samples H_m would also affect the quality of classification. For example, if H_m is set too small, it is hard to comprehensively describe the recent driving intentions through the insufficient information. In contrast, an overlarge H_m may contain the redundant information that is

irrelevant to the recent driving changes, increasing the risk of mis-classifications. Therefore, N_c and H_m should be carefully tuned before online applications.

4.1.2. Influence on prediction accuracy by H_m and N_c

The settings on N_c and H_m would affect the quality of driving sample clustering, thus further influencing the velocity prediction performance. To find the proper settings on N_c and H_m, the MC predictor with different (N_c, H_m) candidates is tested on the combined testing cycle (including all speed profiles in Fig. 5(a)). Fig. 5(e) presents the average RMSE results ($H_p = 5$). As can be seen, the highest prediction accuracy is achieved when $N_c = 4$ and $H_m = 5$. Moreover, Fig. 5(f) presents an example of classification results using such parameter setting. For better graph readability, each class of speed samples in moving horizons is marked with a specific color and the samples in different moving horizons are separated with offset. As can be seen, speed samples are correctly classified into four states, indicating the vehicles' related operation stages. Hence, it can be confirmed that when $N_c = 4$ and $H_m = 5$, the original database can be properly separated into multiple sub-databases through the proposed data structure $[V_{ave}, V_{std}, A_{ave}]$. Note such parameter setting is adopted for the FCM-MC predictor.

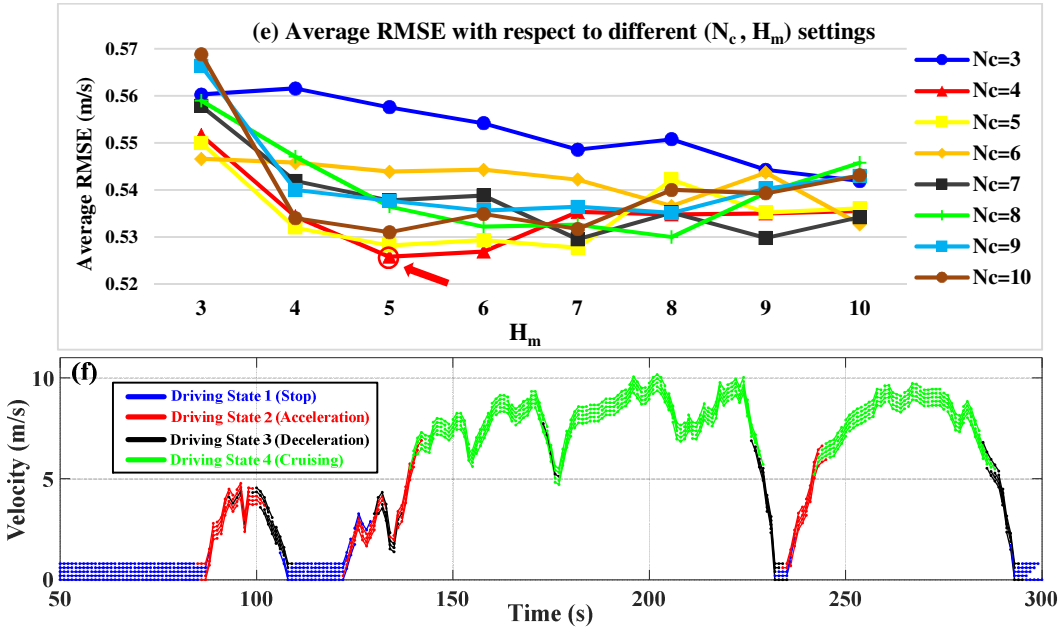

Fig. 5(e). Average RMSE ($H_p = 5$) on the testing cycle under different (N_c, H_m) settings. (f). Example of classification results when $N_c = 4$ and $H_m = 5$.

4.1.3. Comparison with benchmark predictors

A comparative study is conducted to evaluate the performance of FCM-MC predictor. Specifically, two benchmark predictors are introduced, including a conventional multi-step Markov Chain predictor (MSMC) and a back-propagation neural network predictor (BPNN).

- **Benchmark predictor description**

Compared to the FCM-MC predictor, the TPM group of MSMC predictor is estimated based on the original driving database without preprocessing by the FCM technique. Please note the number of MC state is set to 50. Additionally, based on the NN parameter setting suggestions [21], a three-layer BPNN predictor is adopted as the benchmark. Specifically, 85% of original driving data is used as the BPNN training sample while the left 15% is used for performance validation.

- **Prediction performance comparison**

Another speed profile for mail delivery (marked as CYCLE_I) is used as the testing cycle, as depicted in Fig. 6(a). Specifically, Fig. 6(b)-(d) display the detail prediction results of three methods ($H_p = 5$), where the prediction results of MSMC approach tend to diverge dramatically from the actual speed profile, leading to the worst performance among all predictors. This is because the MSMC predictor characterizes the future velocity distributions only based on the current driving state, making it hard to describe the blended and changeable driving behaviors. In contrast, when using more historical driving data for prediction, the BPNN predictor characterizes the future velocity distributions in a more convincing manner, leading to the quality enhancement of prediction.

Additionally, as depicted in Fig. 6(d1) and (d2), the FCM-MC predictor outperforms the benchmark predictors in terms of the overall prediction accuracy. Besides, it exhibits a quicker re-convergence rate after the speed inflection points, as highlighted in the dashed rectangle regions within each subfigure. The reason for such performance improvement is: (1) based on the identification results of recent driving states, proper predictive sub-models are adopted for online speed forecasting; (2) by aggregating the forecasted speed profiles from all sub-models with the quantified fuzzy membership degrees, the proposed method has a certain level of robustness towards the mis-identification of input driving states.

Similarly, the comparative studies are also conducted under other four testing cycles, namely CYCLE_II to CYCLE_V. Table 3 summarizes the average RMSE of all predictors, where the FCM-MC predictor results in the highest prediction accuracy among three approaches under five testing cycles. Specifically, compared to the MSMC approach, the average prediction accuracy improvement by the FCM-MC predictor are respectively 9.31% (Hp = 5) and 14.57% (Hp = 10). Besides, compared with the BPNN predictor, the FCM-MC can reduce the average prediction error by 10.24% (Hp = 5) and 9.87% (Hp = 10), respectively. Therefore, it can be confirmed that the FCM-MC predictor can improve the quality of speed prediction compared to benchmark approaches.

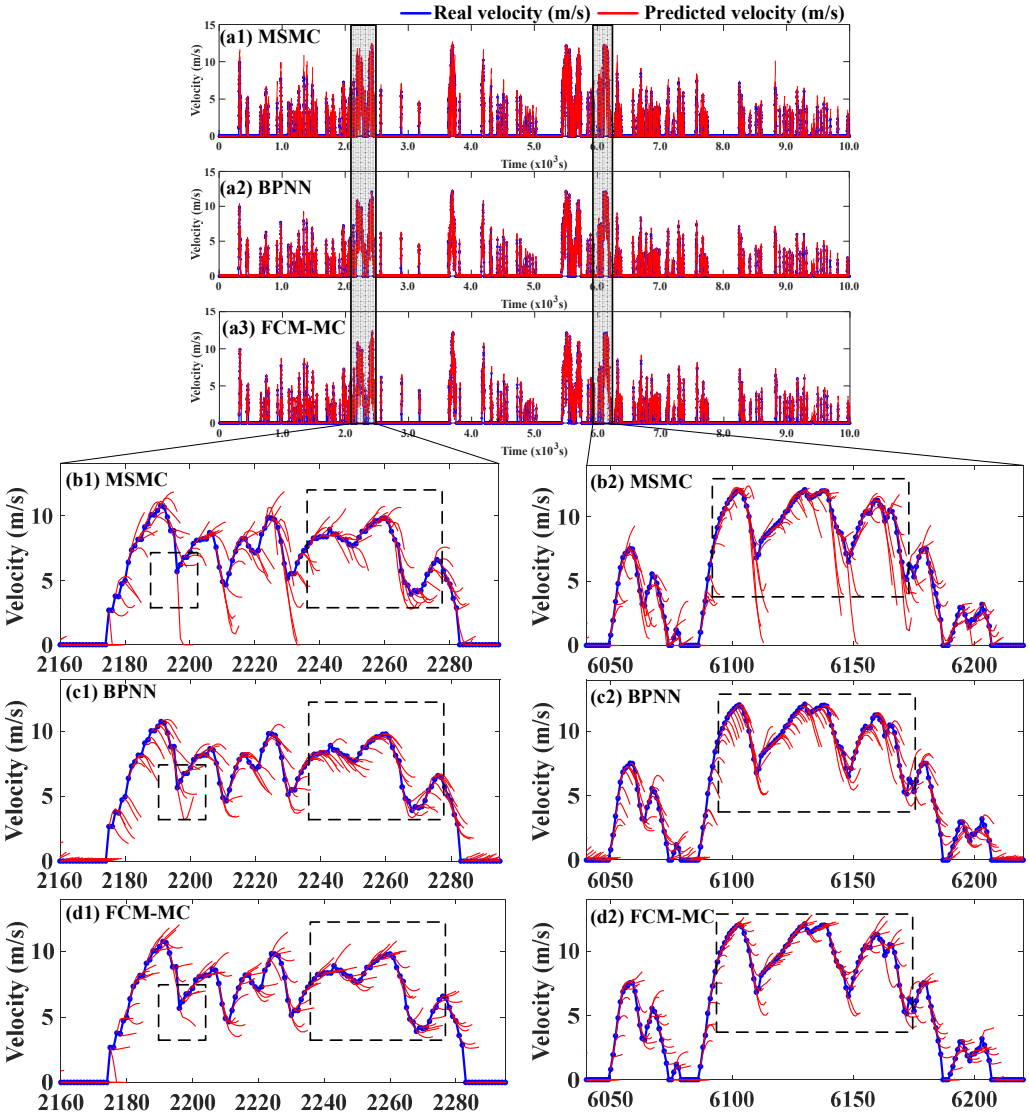

Fig. 6. Speed forecasting performance evaluation on CYCLE_I (H_p = 5): (a) global view of prediction results, (b) performance of conventional multi-step Markov predictor (MSMC), (c) performance of back propagation neural network (BPNN) predictor and (d) performance of fuzzy C-means based Markov predictor (FCM-MC).

TABLE 3. Average RMSE (m/s) of three predictors under five testing cycles.

Items	CYCLE_I		CYCLE_II		CYCLE_III		CYCLE_IV		CYCLE_V	
H_p	5s	10s	5s	10s	5s	10s	5s	10s	5s	10s
MSMC	0.5100	0.8289	0.5750	0.9224	0.6193	0.9896	0.5710	0.9240	0.5518	0.8876
BPNN	0.5263	0.8072	0.5860	0.8920	0.6192	0.9481	0.5801	0.8940	0.5533	0.8232
FCM-MC	**0.4569**	**0.6937**	**0.5272**	**0.7985**	**0.5685**	**0.8558**	**0.5236**	**0.7972**	**0.4976**	**0.7472**

4.2. Evaluation on predictive energy management strategy

Combined with the FCM-MC predictor and the adaptive SoC reference generator, the MPC-based PEMS is compared against the benchmark EMSs in this subsection.

4.2.1 Selection of fuel cell reference working point

To improve the overall FCS working efficiency, the fuel cell reference working point $P_{FC_{ref}}$ should be carefully pre-determined. To cover the vehicles' daily driving conditions, the speed profiles of 12 mail delivery tasks are used for $P_{FC_{ref}}$ extraction. As a powerful technique in search for the global optima, DP is used to extract the FCS working points, where the global optimization problem is formulated as follows:

$$\min_{\Delta P_{FC} \in \mu_{FC}} \sum_{k=0}^{N-1} \Delta m_{H_2}\left(\Delta P_{FC}(k)\right) \cdot \Delta T \tag{16a}$$

$$s.t. \begin{cases} 0.3 \le SoC(k) \le 0.9 & (16b) \\ 0 \le P_{FC}(k) \le 1200\ W & (16c) \\ -40\ W/s \le \Delta P_{FC}(k) \le 40\ W/s & (16d) \\ -10\ kW \le P_{BAT}(k) \le 30kW & (16e) \\ SoC_0 = 0.45, P_{FC_0} = 0\ W & (16f) \\ SoC_N = 0.3 & (16g) \end{cases}$$

where N is the duration of each mail delivery task. The FC power changing rate ΔP_{FC} is picked as the manipulated variable and μ_{FC} represents the discretized domain of ΔP_{FC} with grid resolution of 1 W/s. Additionally, the SoC, FC power, FC power transients and battery power are restricted within their permissible boundaries by (16b)-(16e). Constraint (16f) defines the initial states of battery SoC and FC power. (16g) denotes the terminal SoC constraint. To emphasize the function of FCS as a range extender, SoC_0 is set as 0.45 to simulate the situations when the battery is not fully charged. Please note that the FC reference working points under other SoC_0 settings can be extracted in the same way.

As shown in Fig. 7, 81.22% DP-optimized FC working points are distributed within the high efficiency region. Consequently, the median value is selected as the reference FC power for online application, namely $P_{FC_{ref}} = 550\ W$.

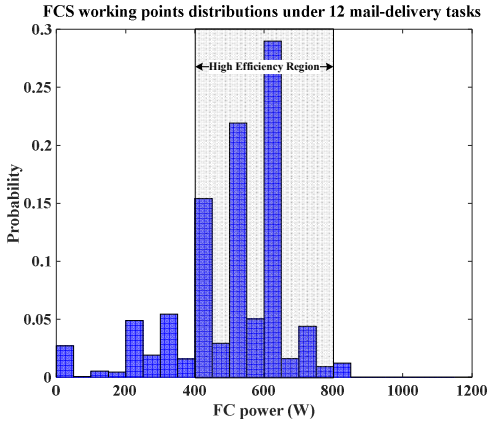

Fig. 7. The P_{FC} distribution under 12 mail-delivery tasks.

4.2.2 Analysis of different impact factors

To explore the potential impacts on EMS performance brought by several parameters (e.g. k_ρ and H_p etc.), a postal delivery mission profile as shown in Fig. 8(a) is used as the testing cycle.

- **Battery SoC regulation performance with different k_ρ**

As stated before, the positive constant k_ρ defines the upper boundary of the adjusting factor ρ, which could bring significant impacts on the SoC regulation performance. Therefore, a proper k_ρ should be predetermined. With $H_p = 5$ and different k_ρ candidates, the proposed MPC-based EMS is verified on the testing cycle and the corresponding battery SoC profiles are depicted in Fig. 8(b). Among k_ρ candidates (1 to 6), a larger k_ρ would accelerate the overall battery energy depletion rate, making the terminal battery SoC closer to the threshold (0.3). However, using an overlarge k_ρ (e.g. $k_\rho = 5,6$) would lead to the occurrence of SoC urgency event (SoC < 0.3) before the end of the trip, resulting in the prolonged CS driving phase. To tradeoff between the battery energy utilization rate and the battery operation safety, k_ρ is set to four.

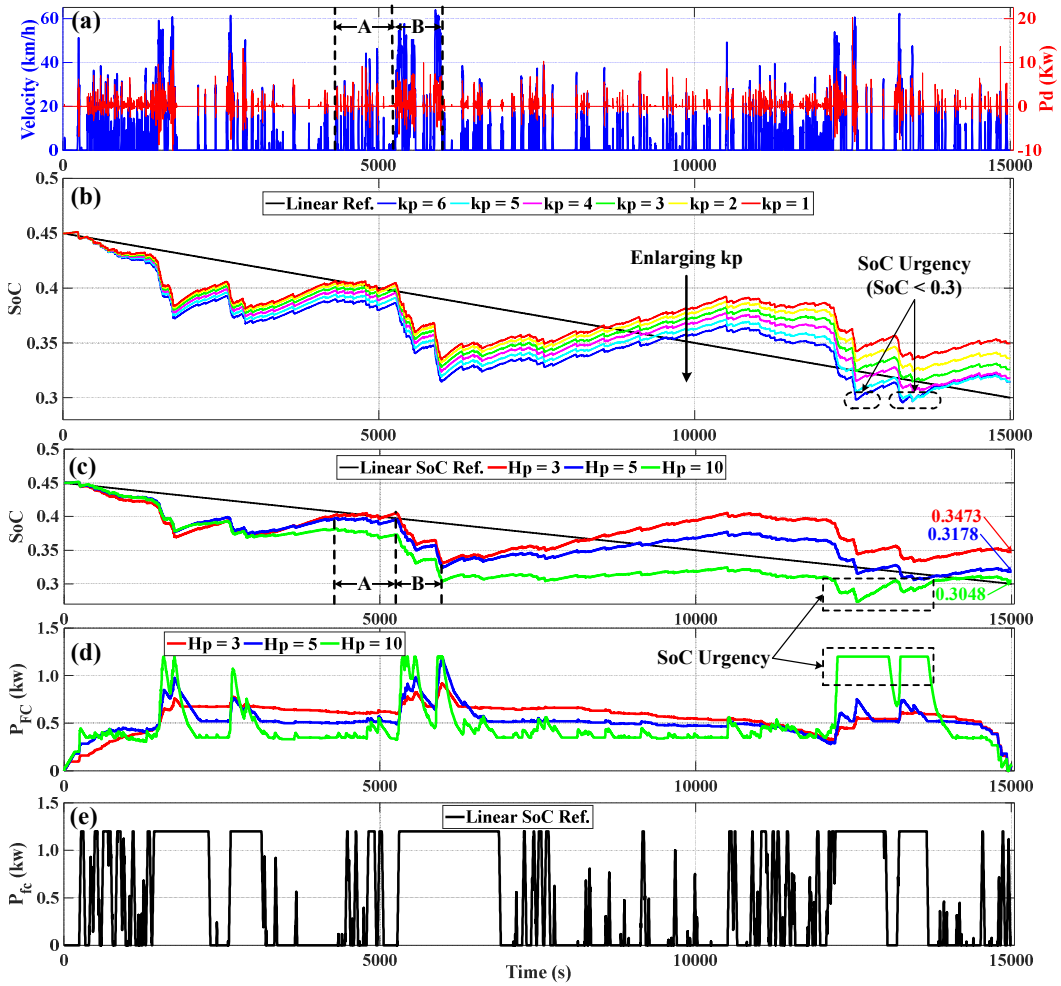

Fig. 8. EMS performance comparison against various impact factors. (a) The speed (blue) and power demand profiles (red) of the used testing cycle. (b) SoC trajectories with different k_ρ ($H_p = 5$). (c) SoC trajectories with different H_p ($k_\rho = 4$). (d) FC power profiles with the proposed adaptive SoC reference. (e) FC power profile with linear SoC reference.

- **Comparison between adaptive SoC reference and linear SoC reference**

To compare the SoC regulation performance between the adaptive SoC reference (7) and the existing linear SoC reference [23], the MPC-based EMS (with $k_\rho = 4$ and different H_p (3s, 5s and 10s)) is performed on the testing cycle, where the related SoC profiles are shown in Fig. 8(c). Specifically, increasing H_p makes the final SoC closer to the target value (0.3), indicating a deeper battery discharge. Moreover, the linear SoC reference leads to a constant energy depletion rate along the entire cycle. In contrast, the adaptive SoC reference model can regulate the actual SoC depleting rates regarding changeable driving conditions. For example, a lower SoC depleting rate appears under the congested driving conditions (e.g. phase A), while a higher SoC depleting rate occurs during the flowing driving conditions (e.g. phase B). Consequently, the adaptive SoC reference generator enables a flexible battery

energy usage towards various power requirements, thus improving the rationality in energy allocation against the linear SoC reference.

- **Fuel cell power performance comparison with different SoC references**

Fig. 8(d) and (e) depict the FCS power profiles tracking the adaptive SoC reference and the linear SoC reference, respectively. When tracking the adaptive SoC reference, increasing H_p would decrease the average of FC power, which is beneficial to reduce the H2 consumption. However, the FCS would work more actively in this case, leading to larger power transients. In contrast, as shown in Fig. 8(e), extremely large FC power spikes as well as frequent start-stop cycles occur when tracking the linear SoC reference, which would greatly shorten the lifetime of FCS. Additionally, as highlighted in the dashed regions in Fig. 8(c) and (d), when H_p =10 and SoC < 0.3, the SoC emergency mode is activated, where the FCS is working towards its maximum power point (1.2kW) to help SoC back to the safe operation range [0.3, 0.9].

- **Determination of prediction horizon**

Table 4 summarizes the EMS performance discrepancies with different H_p, where m_{H_2} is the amount of H2 that is actually consumed. To acquire the convincing comparison results on fuel economy, the final SoC (SoC_{end}) deviation from 0.3 is transformed into the equivalent H2 consumption ($m_{H_2}^{equ}$) [9]. Specifically, enlarging H_p could increase $m_{H_2}^{equ}$ but lead to a deeper battery discharge. Meanwhile, the average FC power transients ($\overline{|\Delta P_{fc}|}$) and the computation time per step (T_{cal}) would also be increased through a larger H_p. Therefore, H_p = 5 is a reasonable choice to tradeoff among the fuel economy, the FC power transients and the computation efficiency.

TABLE 4. MPC-based EMS performance under testing cycle with different H_p.

Prediction Horizon (s)	m_{H_2} **(g)**	$m_{H_2}^{equ}$ **(g)**	SoC_{end}	$\overline{\lvert\Delta P_{fc}\rvert}$ **(W/s)**	T_{cal} **(ms)**
3	99.4	87.2	0.3473	0.6	15.38
5	92.5	87.9	0.3178	1.0	16.73
10	90.2	89.0	0.3048	1.8	22.04

4.2.3. Comparison with benchmark energy management strategies

To further verify the performance of the proposed EMS, two benchmark EMSs are introduced for comparison. As the upper benchmark, DP extracts the optimal fuel cell power profiles based on the fully

previewed trip information, as formulated by (16). In contrast, the MPC controller with the linear SoC reference is regarded as the lower benchmark, marked as "L-MPC". Besides, the proposed EMS with the adaptive SoC reference (7) is marked as "A-MPC". For both MPC-based strategies, $H_p = 5$ and $k_\rho = 4$.

- **EMS performance comparison with benchmark strategies**

Five GPS-collected speed profiles for mail-delivery are employed for validating the EMSs, where the related comparison results under two mission profiles are detailed in Fig. 8(f)-(k).

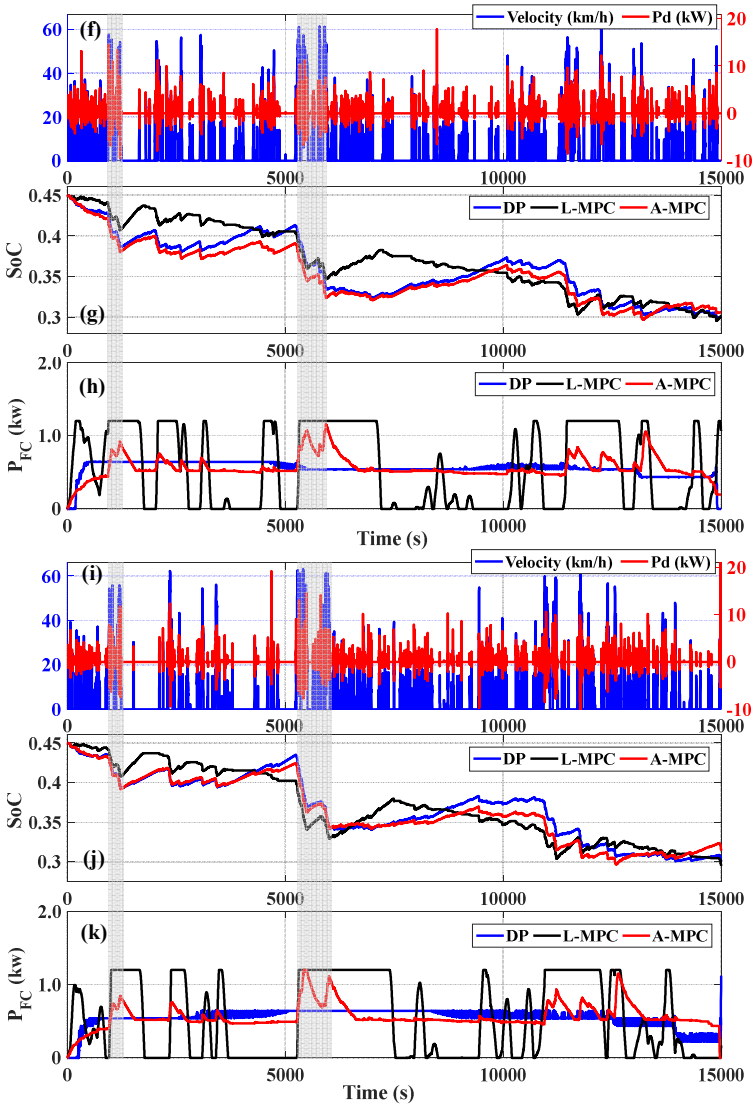

Fig. 8. EMS performance comparison with benchmark strategies. (f) Speed (red) and power demand (blue) profiles of testing cycle I. (g) SoC profiles of different EMSs on testing cycle I. (h) Fuel cell power profiles of different EMSs on testing cycle I. (i) Speed (red) and power demand (blue) profiles of testing cycle II. (j) SoC profiles of different EMSs on testing cycle II. (k) Fuel cell power profiles of different EMSs on testing cycle II.

As shown in Fig. 8(g) and (j), under both testing cycles, A-MPC can effectively regulate the SoC depleting rate against the changeable driving conditions, where its SoC profiles are close to the DP-based

ones. Besides, given the linear SoC reference, the L-MPC tends to maintain the constant SoC depleting rate along the driving cycle. However, due to the maximum FC power limits, the SoC profiles of L-MPC deviate from the linear reference in some peaking power regions (marked with the grey shadow). Moreover, as depicted in Fig. 8(h) and (k), benefiting from the fully previewed trip information, DP manipulates the FCS with the fewest power transients. In contrast, L-MPC regulates the FCS power in an aggressive manner, where much larger power spikes and many start-stop cycles are observed. In contrast, A-MPC is able to smooth the FC power profiles, showing the great potential in extending the FCS's lifetime.

Furthermore, Fig. 8(l) and (m) depicts the corresponding FC working point distributions. Specifically, 97.54% (testing cycle I) and 90.66% (testing cycle II) of FC working points for DP are located in the high efficiency region, while this ratio for L-MPC under both testing cycles are respectively 7.51% and 9.12%. In contrast, A-MPC can improve this ratio to 86.39% (testing cycle I) and 85.56% (testing cycle II). This indicates the proposed EMS can greatly enhance the FCS working efficiency compared to L-MPC strategy.

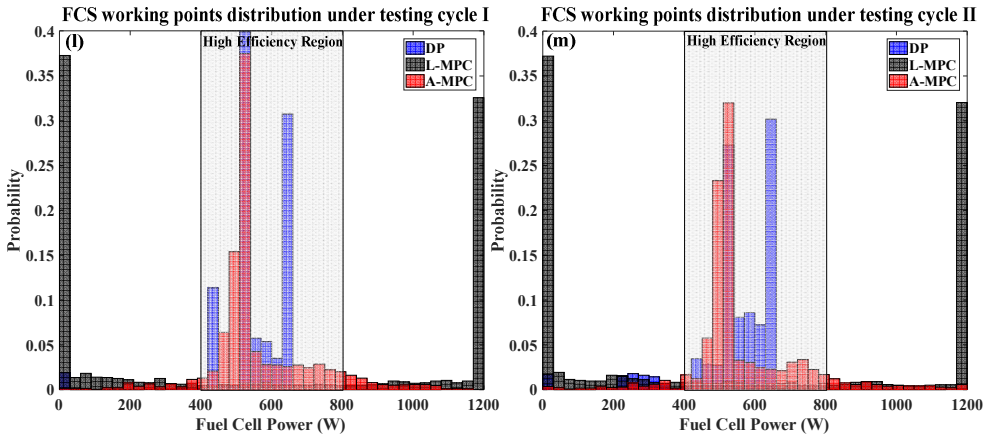

Fig. 8(l) and (m). FCS working points probability distributions under two testing cycles.

Table 5 summarizes the EMS performances under five testing cycles, where r_{high} denotes the ratio of FCS working within the high efficiency region. Specifically, at least 70.46% FCS working points of A-MPC are distributed within the high efficiency area, where the enhanced working efficiency leads to 3.79% to 5.35% reduction of equivalent H2 consumption ($m_{H_2}^{equ}$) compared to the L-MPC benchmark. Besides, A-MPC can also decrease the average FC power transients ($\overline{|\Delta P_{fc}|}$) by 40.4% to 54.7% compared to L-

MPC, thus enhancing the FCS's durability. Furthermore, A-MPC performs close to DP benchmark under five testing cycles, where the largest performance gap on $m_{H_2}^{equ}$ and $\overline{|\Delta P_{fc}|}$ are respectively 0.84% (testing cycle II) and 9.18% (testing cycle V). In addition, the online calculation time per step (T_{cal}) for A-MPC ranges from 16.53 ms to 16.77 ms, which is sufficiently smaller than the sampling time interval (1s), making it suitable for real-time applications.

TABLE 5. EMS performance evaluation results under five testing cycles.

	Testing cycle I			**Testing cycle II**			**Testing cycle III**		
	DP	**L-MPC**	**A-MPC**	**DP**	**L-MPC**	**A-MPC**	**DP**	**L-MPC**	**A-MPC**
m_{H_2}**(g)**	96.9	102.1	**99.3**	95.1	98.8	**99.6**	73.8	78.5	**80.6**
$m_{H_2}^{equ}$ **(g)**	96.9	101.7	**97.7**	95.1	100.1	**95.9**	73.8	78.5	**74.3**
SoC_{end}	0.3000	0.3016	**0.3063**	0.3000	0.2953	**0.3142**	0.3000	0.2999	**0.3243**
$\overline{\lvert\Delta P_{fc}\rvert}$ **(W/s)**	0.96	2.25	**1.02**	0.97	2.24	**1.04**	0.85	1.61	**0.87**
r_{high}	97.54%	7.51%	**86.39%**	90.66%	9.12%	**85.56%**	95.39%	11.69%	**70.46%**
T_{cal} **(ms)**	---	16.97	**16.63**	---	16.67	**16.58**	---	16.75	**16.62**
	Testing cycle IV			**Testing cycle IV**					
	DP	**L-MPC**	**A-MPC**	**DP**	**L-MPC**	**A-MPC**			
m_{H_2}**(g)**	100.8	105.5	**109.5**	98.6	102.8	**102.7**			
$m_{H_2}^{equ}$ **(g)**	100.8	105.9	**101.5**	98.6	103.0	**99.1**			
SoC_{end}	0.3000	0.2983	**0.3308**	0.3000	0.2993	**0.3139**			
$\overline{\lvert\Delta P_{fc}\rvert}$ **(W/s)**	0.98	1.71	**1.02**	0.98	2.33	**1.07**			
r_{high}	79.75%	6.65%	**78.87%**	89.09%	11.13%	**83.33%**			
T_{cal} **(ms)**	---	16.69	**16.77**	---	16.75	**16.53**			

- **Sensitivity analysis under trip duration estimation errors**

In this work, the scheduling of battery energy usage is achieved based on the assumption that the trip duration T_{trip} on the mail-delivery routes can be estimated before departure. However, considering the complex traffic conditions in reality (e.g. stochastic distributions of the traffic lights etc.), the actual trip duration would deviate from the estimated ones to some extent. To explore the potential impacts on the EMS performance brought by trip duration estimation errors, a sensitivity analysis is presented, where different levels of estimation errors (-30% to 30% of the actual trip duration) are given to the adaptive SoC reference model (7). Please note that the negative errors mean T_{trip} in (7) is smaller than the actual trip duration, while positive errors denote the opposite. Based on trip duration errors, the proposed EMS is evaluated under testing cycle I and II, where the numerical evaluation results are summarized in table 6.

TABLE 6. EMS performance under -30% to 30% trip duration errors.

Testing cycle I						Testing cycle II					
Error	m_{H_2} **(g)**	$m_{H_2}^{equ}$ **(g)**	SoC_{end}	$\overline{\lvert\Delta P_{fc}\rvert}$ **(W/s)**	r_{high}	**Error**	m_{H_2} **(g)**	$m_{H_2}^{equ}$ **(g)**	SoC_{end}	$\overline{\lvert\Delta P_{fc}\rvert}$ **(W/s)**	r_{high}
-30%	99.4	99.0	0.3015	1.35	53.69%	-30%	96.4	97.5	0.2958	1.34	54.50%
-20%	98.9	98.5	0.3013	1.48	63.05%	-20%	95.9	97.0	0.2960	1.57	62.96%
-10%	98.4	98.2	0.3010	1.32	77.93%	-10%	95.3	96.7	0.2947	1.24	73.92%
0%	99.3	97.7	0.3063	1.02	86.39%	0%	99.6	95.9	0.3142	1.04	85.55%
10%	99.8	97.6	0.3086	0.98	86.90%	10%	99.9	95.9	0.3129	0.97	86.49%
20%	100.6	97.6	0.3102	0.98	86.60%	20%	100.0	95.8	0.3164	0.98	86.22%
30%	101.1	97.6	0.3143	0.98	86.50%	30%	100.6	95.8	0.3185	0.98	87.86%

Specifically, the trip duration errors would bring different impacts on following performance metrics:

- **Fuel economy**

If positive errors are applied when planning battery energy usage, the actual SoC depleting rate would be reduced by the enlarged T_{trip}, leading to the larger SoC_{end} under both testing cycles. In this case, larger portion of power demand would be supplied by the FCS, thus increasing the amount of actual H2 consumption (m_{H_2}). Besides, r_{high} remains almost the same under positive errors, indicating the relatively stable FCS working efficiency. Therefore, compared to the zero-error working conditions, the discrepancies on the equivalent H2 consumption ($m_{H_2}^{equ}$) are not significant.

In contrast, negative trip duration estimation errors would accelerate the SoC depletion, making the energy stored in the battery pack fully depleted before the end of the trip, resulting in the smaller SoC_{end}. However, the prolonged CS driving phases would greatly reduce the average FCS working efficiency and thus increase the amount of equivalent H2 consumption. Overall, in face of $\pm$ 30% trip duration estimation errors, the proposed EMS (A-MPC) can still save over 2.65% (testing cycle I) and 1.32% (testing cycle II) equivalent H2 consumption compared to the L-MPC strategy.

- **FCS durability**

When positive trip duration estimation errors appear, the average FC power transients $\left|\overline{P_{fc}}\right|$ slightly decrease compared to the zero-error conditions. This is because the enlarged T_{trip} would shorten or eliminate the CS driving phases, making FCS working more stably, thus reducing the average power transients. In contrast, the extended CS driving phases caused by the negative errors require FCS working more actively to cope with the occurrence of SoC urgency events, thus increasing the FCS power transients. As a result, compared to the L-MPC strategy, over 34.22% (testing cycle I) and 29.91% (testing

cycle II) decrement on the average FCS power transients can be achieved by the A-MPC strategy even with ± 30% trip duration estimation errors.

As a conclusion, the sensitivity analysis results indicate that the proposed EMS has certain level of robustness against the trip duration estimation errors, thus further demonstrating its practicality.

Section V. Conclusion

In this work, an energy management strategy is developed for light-duty plug-in hybrid electric vehicles powered by battery and fuel cell. Specifically, a fuzzy C-means enhanced multi-step Markov velocity forecasting method is proposed. Subsequently, an adaptive SoC reference generation method is devised for planning the battery energy usage. Combined with the speed forecasting results and the SoC reference, the model predictive controller can make proper energy distribution decisions by minimizing the multi-criteria performance index per sampling time step. The major contributions of this work are summarized as:

- The fuzzy C-means clustering technique is adopted to preprocess the original driving database, leading to the generation of multiple Markov predictive sub-models, where each sub-model characterizes the future velocity distribution of specific type of input driving states. At the online application stage, to reduce the negative impacts caused by the uncertainty of driving state identification, the final prediction results are obtained by synthesizing the forecasted speed profiles from all sub-models with the real-time quantified fuzzy membership degrees. Moreover, validation results have demonstrated the improved prediction accuracy and robustness of the proposed predictor against benchmark predictors.
- Benefiting from the velocity prediction results and the estimated trip duration, the adaptive SoC reference generator can regulate the actual SoC depleting rate against different driving conditions, which exhibits a more reasonable battery energy distribution performance compared to the existing linear SoC reference.
- Compared with the lower benchmark strategy, the presented EMS can effectively bring down the vehicle's operation costs through saving H2 consumption (by at least 3.79%) and limiting the FC power spikes (by at least 40.4%), implying the improved fuel economy and a better FCS durability.

Additionally, the proposed strategy performs close to the upper benchmark (DP), where the largest gaps against the global optimality are respectively 0.84% (fuel economy) and 9.18% (fuel cell power transients). Moreover, it is verified that the proposed strategy is robust to certain level of trip duration estimation errors, which is favorable to the real applications.

Acknowledgement

This work has gained supports from China Scholarship Council (CSC) and EIPHI Graduate School (contract "ANR-17-EURE-0002"). Besides, the authors also want to thank the European funded "Mobypost" project (Grant agreement ID: 256834, http://mobypost-project.eu/) for the permission of using the related database.

Reference

[1]. X. Wu, X. Hu, X. Yin, L. Li, Z. Zeng, V. Pickert, Convex programming energy management and components sizing of a plug-in fuel cell urban logistics vehicle, ***Journal of Power Sources***, Vol. 423, May. 2019, Pages 358-366.

[2]. Y. Liu, W. Lehnert, H. Janßen, R. C. Samsun, D. Stolten, A review of high-temperature polymer electrolyte membrane fuel-cell (HT-PEMFC)-based auxiliary power units for diesel-powered road vehicles, ***Journal of Power Sources***, Vol. 311, Apr. 2016, Pages 91-102.

[3]. R. Ma, T. Yang, E. Breaz, Z. Li, P. Briois, F. Gao. Data-driven proton exchange membrane fuel cell degradation predication through deep learning method. ***Applied Energy***, Vol. 231, Pages: 102-115, Dec. 2018.

[4]. W. Zhou, L. Yang, Y. Cai, T. Ying, Dynamic programming for new energy vehicles based on their work modes Part II: Fuel cell electric vehicles, ***Journal of Power Sources***, Vol. 407, Dec. 2018, Pages 92-104.

[5]. H. Marzougui, A. Kadri, J. Martin, M. Amari, S. Piefederici, F, Bacha. Implementation of energy management strategy of hybrid power source for electrical vehicle. ***Energy Conversion and Management***, Vol. 195, Pages: 830-843, Sep. 2019.

[6]. M. Sorrentino, V. Cirillo, L. Nappi. Development of flexible procedures for co-optimizing design and control of fuel cell hybrid vehicles. ***Energy Conversion and Management***, Vol. 185, Pages: 537-551, Apr. 2019.

[7]. J. P. Trovao, C.H. Antunes. A comparative analysis of meta-heuristic methods for power management of a dual energy storage system for electric vehicles. ***Energy Conversion and Management***, Vol. 95, Pages: 281-296, May. 2015.

[8]. A. Ravey, B. Blunier, A. Miraoui. Control Strategies for Fuel-Cell-Based Hybrid Electric Vehicles: From Offline to Online and Experimental Results. ***IEEE Transactions on Vehicular Technology***. Vol. 61(6), Page: 2452-2457. May 2012.

[9]. D. Zhou, A. Al-Durra, F. Gao, A. Ravey, I. Matraji, M. G. Simões. Online energy management strategy of fuel cell hybrid electric vehicles based on data fusion approach. ***Journal of Power Sources***. Vol. 366, Page: 278-291, Oct 2017.

[10]. K. Song, F. Li, X. Hu, L. He, W. Niu, S. Lu, T. Zhang, Multi-mode energy management strategy for fuel cell electric vehicles based on driving pattern identification using learning vector quantization neural network algorithm, ***Journal of Power Sources***, Vol. 389, Jun. 2018, Pages 230-239.

[11]. W. Zhou, L. Yang, Y. Cai, T. Ying, Dynamic programming for New Energy Vehicles based on their work modes part I: Electric Vehicles and Hybrid Electric Vehicles, ***Journal of Power Sources***, Vol.406, Dec. 2018, Pages 151-166.

[12]. C.H. Zheng, G.Q. Xu, Y.I. Park, W.S. Lim, S.W. Cha, Prolonging fuel cell stack lifetime based on Pontryagin's Minimum Principle in fuel cell hybrid vehicles and its economic influence evaluation, ***Journal of Power Sources***, Vol. 248, Feb. 2014, Pages 533-544.

[13]. Z. Chen, C. C. Mi, B. Xia, C. You, Energy management of power-split plug-in hybrid electric vehicles based on simulated annealing and Pontryagin's minimum principle, ***Journal of Power Sources***, Vol. 272, Dec. 2014, Pages 160-168.

[14]. F. Odeim, J. Roes, A. Heinzel. Power Management Optimization of a Fuel Cell/Battery/Supercapacitor Hybrid System for Transit Bus Applications. ***IEEE Transactions on Vehicular Technology***. Vol. 65(7), Pages: 5783-5788. July 2015.

[15]. H. Li, A. Ravey, A. N'Diaye, A. Djerdir, A novel equivalent consumption minimization strategy for hybrid electric vehicle powered by fuel cell, battery and supercapacitor, ***Journal of Power Sources***, Vol. 395, Pages: 262-270, Aug. 2018.

[16]. T. Wang, Q. Li, Y. Qiu, L. Yin, L. Liu and W. Chen, Efficiency Extreme Point Tracking Strategy Based on FFRLS Online Identification for PEMFC System, ***IEEE Transactions on Energy Conversion***, vol. 34 (2), pp. 952-963, June 2019.

[17]. T. Li, H. Liu, D. Ding. Predictive energy management of fuel cell supercapacitor hybrid construction equipment. ***Energy***, 149 (2018), pp. 718-729.

[18]. Y. Zhou, A. Ravey, MC. Péra, Multi-mode predictive energy management for fuel cell hybrid electric vehicles using Markov driving pattern recognizer, ***Applied Energy***, Vol. 258, 2020, 114057.

[19]. H. Wang, Y. Huang, A. Khajepour, Q. Song. Model predictive control-based energy management strategy for a series hybrid electric tracked vehicle. ***Applied Energy***, Vol. 182, Page: 105-114. Nov. 2016.

[20]. C. Sun, S. J. Moura, X. Hu, J. Hedrick, F, Sun. Dynamic Traffic Feedback Data Enabled Energy Management in Plug-in Hybrid Electric Vehicles. ***IEEE Transactions on Control System Technology***, Vol. 23(3), May 2015.

[21]. C. Sun, X. Hu, S. J. Moura, F. Sun. Velocity Predictors for Predictive Energy Management in Hybrid Electric Vehicles. ***IEEE Transactions on Control System Technology***, Vol. 23(3), May 2015.

[22]. Y. Huang, H. Wang, A. Khajepour, H. He, J. Ji. Model predictive control power management strategies for HEVs: A review. ***Journal of Power Sources***, 341 (2017), pp. 91-106.

[23]. G. L, J. Zhang, H. He. Battery SOC constraint comparison for predictive energy management of plug-in hybrid electric bus. ***Applied Energy***, Vol. 194, May 2017, Pages 578-587.

[24]. S. Xie, X. Hu, Z. Xin, J. Brighton. Pontryagin's Minimum Principle based model predictive control of energy management for a plug-in hybrid electric bus. ***Applied Energy***, Vol.236, Pages: 893-905, Feb. 2019.

[25]. X. Li, Y. Wang, D. Yang, Z. Chen. Adaptive energy management strategy for fuel cell/battery hybrid vehicles using Pontryagin's Minimal Principle. ***Journal of Power Sources***, Vol. 440, 227105, Nov. 2019.

[26]. J. Guo, H. He, J. Peng, N. Zhou. A novel MPC-based adaptive energy management strategy in plug-in hybrid electric vehicles. ***Energy***, Vol. 175, Pages: 378-392, May, 2019.

[27]. Z. Chen, N. Guo, J. Shen, R. Xiao and P. Dong. A Hierarchical Energy Management Strategy for Power-Split Plug-in Hybrid Electric Vehicles Considering Velocity Prediction. ***IEEE Access***, vol. 6, pp. 33261–33274, 2018.

[28]. S. Xie, X. Hu, S. Qi, K. Lang. An artificial neural network-enhanced energy management strategy for plug-in hybrid electric vehicles. ***Energy***, Vol.163, Pages: 837-848, Nov. 2018.

[29]. Y. Zhou, A. Ravey, MC. Péra. A survey on driving prediction techniques for predictive energy management of plug-in hybrid electric vehicles. ***Journal of Power Sources***. Vol. 412 (2019), pp. 480-495.

[30]. J. Jing, D. Filev, A. Kurt, E. Ozatay, J. Michelini, U. Ozguner. Vehicle speed prediction using a cooperative method of fuzzy Markov model and auto-regressive model. ***2017 IEEE Intelligent Vehicles Symposium (IV)***, Los Angeles, CA, USA, Jul. 2017.

[31]. P. Tulpule, V. Marano, G. Rizzoni. Effects of Different PHEV Control Strategies on Vehicle Performance. ***American Control Conference***. June 2009.

[32]. C. Zheng, G. Xu, K. Xu, Z. Pan, Q. Liang. An energy management approach of hybrid vehicles using traffic preview information for energy saving. ***Energy Conversion and Management***, Vol. 105, Pages: 462-470, Nov.2015.

[33]. H. Tian, Z. Lu, X. Wang, X. Zhang, Y. Huang, G. Tian. A length ratio based neural network energy management strategy for online control of plug-in hybrid electric city bus. ***Applied Energy***, Vol. 177, Page: 71-80. Sep. 2016.

[34]. M. Montazeri-Gh, Z. Pourbafarani. Near-Optimal SOC Trajectory for Traffic-Based Adaptive PHEV Control Strategy. ***IEEE Transactions on Vehicular Technology***. Vol. 66(11), Page 9753 - 9760. Nov. 2017.

[35]. Z. Hu, J. Li, L. Xu, Z. Song, C.Fang, M. Ouyang, G. Dou, G. Kou. Multi-objective energy management optimization and parameter sizing for proton exchange membrane hybrid fuel cell vehicles. ***Energy Conversion and Management***, Vol. 129, Pages: 108-121, Dec. 2016.

[36]. A. Ravey, S. Faivre, C. Higel, F. Harel and A. Djerdir, Energy management of fuel cell electric vehicle with hydrid tanks, ***IECON 2014 - 40th Annual Conference of the IEEE Industrial Electronics Society***, Dallas, TX, 2014, pp. 3962-3967.

[37]. C. Higel, F. Harel, D. Candusso, S. Faivre, A. Ravey, D. Guilbert, A. N' diaye, D. Bouquain, A. Djerdir, A. Gaillard. Part 1: Mobypost vehicle's powertrain modeling, simulation and sizing. ***Conference on Fundamentals and Development of Fuel Cells (FDFC 2013)***, Apr. 2013, Germany.

[38]. L. Guzzella, A. Sciarretta. Vehicle Propulsion Systems: Introduction to Modeling and Optimization. ***Berlin: Springer-Verlag***, pp. 14-18, 2005

[39]. F. Gao, B. Blunier, A. Miraoui and A. El Moudni, A Multiphysic Dynamic 1-D Model of a Proton-Exchange-Membrane Fuel-Cell Stack for Real-Time Simulation, ***IEEE Transactions on Industrial Electronics***, vol. 57, no. 6, pp. 1853-1864, June 2010.

[40]. T Markel, A Brooker, T Hendricks, V Johnson, K Kelly, B Kramer, M O'Keefe, S Sprik, K Wipke, ADVISOR: a systems analysis tool for advanced vehicle modeling, ***Journal of Power Sources***, Volume 110, Issue 2, 2002, Pages 255-266.

[41]. MC. Péra, D. Hissel, H. Gualous, C. Turpin. Electrochemical Components. ***John Wiley & Sons***, Inc. 2013.

[42]. J. C. Bezedek. Pattern recognition with fuzzy objective function algorithms. ***Springer Science & Business Media***. 2013.

[43]. D. P. Filev and I. Kolmanovsky, Generalized markov models for real-time modeling of continuous systems. ***IEEE Transactions on Fuzzy Systems***, vol. 22, no. 4, pp. 983–998, 2014.